Project-thesis

Optimization of the growth conditions of magnetite films on YSZ substrates

by Yifan Xu
of Material Science in RWTH Aachen
October 2021

supervised by

Prof. Dr. Thomas Brückel

in JCNS-2/PGI-4, Forschungszentrum Jülich

Zusammenfassung

Magnetit (Fe_3O_4) ist ein vielversprechender Kandidat für die Spintronik. Als inerter Sauerstofflieferant ist YSZ (Yttria Stabilized Zirconia) ein ideales Substrat, um auf diesem die Wachstumsparameter von Fe_3O_4 zu optimieren. Dieses Projekt umfasst das Züchten und die Charakterisierung von Magnetit auf YSZ-Substraten. Die Magnetit-Wachstumsparameter wurden für den Prozess des Laserstrahlverdampfens (PLD) optimiert und eine Reihe von Proben bei unterschiedlichen Temperaturserie für weitere Untersuchungen hergestellt. Mittels Rasterkraftmikroskopie (AFM) und Röntgenreflektometrie (XRR) wird die Oberflächenmorphologie des Fe_3O_4 untersucht. Röntgenbeugeung (XRD) wird verwendet, um die Kristallinität zu überprüfen und die Gitterkonstante der dünnen Schichten außerhalb der Ebene zu berechnen. Durch Messungen magnetischer und elektrischer Eigenschaften untersuchen wir die Metall-Isolator-Verwey-Übergangstemperatur, die empfindlich von der Magnetit-Stöchiometrie abhängt. Die Analyse des Magnetowiderstands innerhalb der Ebene und außerhalb der Ebene ist außerdem ein Indikator für die kristalline Anordnung von Magnetit auf YSZ-Substraten. Die optimierten Wachstumsparameter werden verwendet, um Magnetit auf Strontium-Titanit-Substraten zu züchten und die Eigenschaften von Fe_3O_4 werden hier durch Glühen und ein angelegtes elektrisches Feld abgestimmt und im Rahmen meiner Masterarbeit mit XRD, weitwinkel-Röntgenstreuung (WAXS) und supraleitendes Quanteninterferenzgeräte (SQUID) charakterisiert.

Abstract

Magnetite (Fe_3O_4) is a promising candidate for spintronics. As an inert oxygen supplier, YSZ (Yttria Stabilized Zirconia) is an ideal substrate for optimizing the growth parameters of Fe_3O_4 on it. This project encompasses the growth and characterization of magnetite on YSZ substrates. Magnetite growth parameters were optimized for Pulsed laser deposition (PLD) and a series of samples was produced at different temperature for further study. Using Atomic force microscopy (AFM) and X-ray reflectometry (XRR), the surface morphology of the Fe_3O_4 is examined. X-ray diffraction (XRD) is used to check the crystallinity and calculate the out-of-plane lattice constant of the thin films. By measuring magnetic and electric properties, we study the metal-insulator Verwey transition temperature which is sensitive to the magnetite stoichiometry. Analyzing the magnetoresistance in-plane and out-of-plane is also an indicator of the crystalline arrangement of magnetite on YSZ substrates. The optimized growth parameters will be used to grow magnetite on strontium titanite substrates and the properties of Fe_3O_4 will here be tuned by annealing and applied electric field and characterized using XRD, wide angle X-ray scattering (WAXS) and superconducting quantum interference device (SQUID) in the framework of my master's thesis.

Contents

1 Introduction and motivation

Information transport is currently based on electronics. With the prosperity of electronics, it consumes huge amounts of energy, which has encouraged people to look into spintronics. The spintronics effect occurs on theoretically 100% spin polarized materials, one of them being half-metallic materials[1]. Half metallic means metallic for one-spin direction and insulating for the other spin direction. Fe_3O_4 is a typical half metal magnetic material. Additionally, Fe_3O_4 has a high Curie temperature around 860K allowing it to be used at room temperature (the details will be discussed in Chapter 2)[2].

YSZ (Yttria stabilized Zirconia) is selected to be the substrate. YSZ doesn't reduce or oxidize Fe_3O_4 thin films, which make it easier to find the optimal growth parameters. However, as a good oxygen conductor, oxygen can be transported from atmosphere through YSZ substrates to Fe_3O_4 thin films. The lattice mismatch of Fe_3O_4 on YSZ is too large to drive the Fe_3O_4 to align in (111) plane. In the result, there is a mismatch of 6% between Fe_3O_4 and YSZ. The growth parameters of Fe_3O_4 are critical, because they can influence its stoichiometry and thus its magnetic properties. Magnetite can be written as $Fe_{3-\sigma}O_4$, with different σ, the properties of magnetite can be influenced. Thus, the influence of different growth parameters on the qualities of Fe_3O_4 thin films grown on YSZ are the focus of this project. We will mainly study on the influence of the laser fluence and the growth temperature.

In chapter 2 the scientific background of lattice structure, magnetic and electric properties of iron oxides will be introduced. Additionally, the important phenomenon – Verwey transition will be discussed. The Verwey transition is a good indicator of the oxygen stoichiometry. Also, we introduce the lattice structure which causes the mismatch between Fe_3O_4 and YSZ and the arrangement of Fe_3O_4 on YSZ. The experimental methods and instruments used for the deposition and characterization of the thin films will be introduced in chapter 3. Finally, the influence of growth parameters (including laser fluency and growth temperature) on the properties of Fe_3O_4 thin films on YSZ substrate will be discussed in chapter4. The morphology will be checked by Atomic force microscopy (AFM), the thickness and roughness of thin films will be calculated from x-ray reflection (XRR) results. The crystalline structure will be characterized using x-ray diffraction (XRD). By using Vibrating sample magnetometry (VSM),

the magnetization is measured depending on magnetic field and measuring temperature. Finally, the electric properties (resistance and magnetoresistance) will be measured by Physical Property Measurement System (PPMS) both in-plane and out-of-plane.

2 Theoretical background

In this study, the major aim is to optimize the growth of the Fe_3O_4 thin films and the interface to the substrate. In this theoretical background section, the properties of magnetite will be first introduced which originates from the different coupling between cations. Thus, different exchange interactions will be introduced. In section 2.2 we will introduce the film growth theory on YSZ substrates.

2.1 Magnetite (Fe_3O_4)- the ferrimagnetic half-metal

With respect to oxygen stoichiometry, different oxides usually have different electric and magnetic properties[3]. For example, Magnetite Fe_3O_4 is a ferrimagnetic half-metal[4]. "Ferrimagnetic" refers to a spontaneous magnetization caused by the different ions Fe^{2+} and Fe^{3+} which are unequal in magnitude. The reduced phase $Fe_{1-x}O$ is an antiferromagnetic insulator. On the other hand, the oxidized phase γ-Fe_2O_3 and α-Fe_2O_3 are ferrimagnetic insulator and antiferromagnetic insulator, respectively. The special properties of Fe_3O_4 originating from the crystal structure will be introduced.

2.1.1 Structure

Fe_3O_4 has a cubic inverse spinel structure[5], with a crystal lattice constant of 8.394 Å, as shown in Figure 2.1. All of the Fe^{2+} ions occupy half of the octahedral sites and the Fe^{3+} are split evenly across the remaining half of octahedral sites and the tetrahedral sites. pattern of occupation of Fe^{2+} and Fe^{3+} cations causes the special ferrimagnetic and electric properties of magnetite as the sublattice with opposite orientation of the magnetic moment.

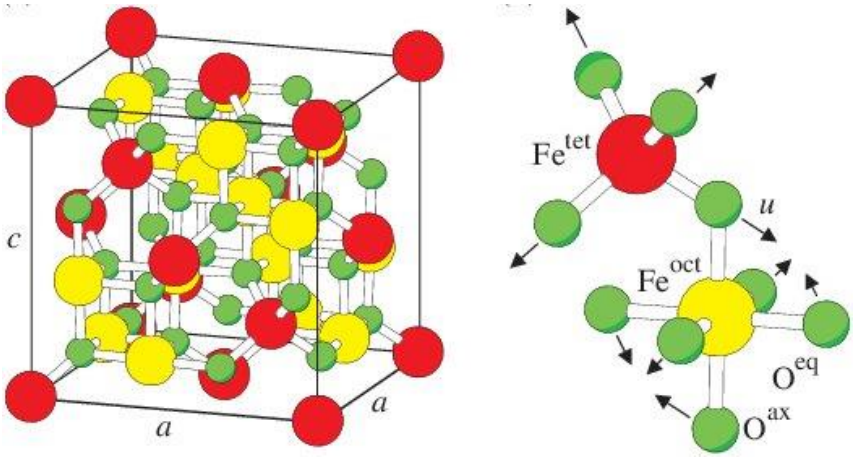

Fig 2.1 Fe_3O_4 crystal structure and the tetrahedra/ Octahedra coordination polyhedron structure(figure taken from ref.[6]).

2.1.2 Properties

Between magnetic cations Fe^{2+} and Fe^{3+} there is not only direct exchange but also the coupling over the oxygen anions[7]. The different ways of coupling through oxygen anions can be defined as super exchange and double-exchange interaction and are shown in Figure 2.2 respectively.

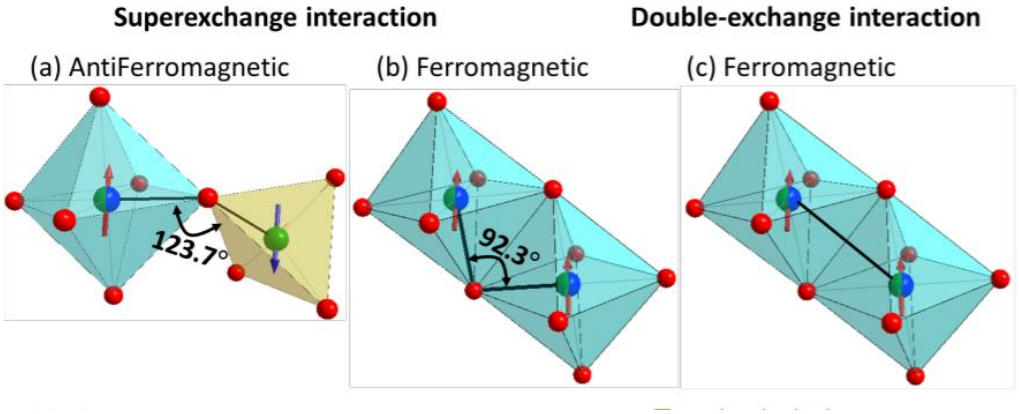

Figure 2.2 Sketch of magnetism in inverse spinel magnetite through first super exchange interaction: (a) the antiferromagnetic coupling between the cations on the T_d (tetrahedral) and on the O_h(octahedral) sites; (b) the ferromagnetic coupling between the cations on the O_h sites. Second, the double-exchange interaction: (c) the ferromagnetic coupling between the O_h sites (figure taken from ref.[8]).

a) Super exchange

Different from direct exchange, super exchange is the strong coupling between two next nearest neighbor cations through a non-magnetic oxygen anion[9-11]. It is caused by the overlap of the

cation d-orbitals and the oxygen p-orbitals. Super exchange interaction can be either ferromagnetic or antiferromagnetic depending on the orbitals and angles between the magnetic ions, which is described by the Goodenough-Kanamori rules[11]:

Antiferromagnetic coupling originates from 180° exchange between filled or empty cation orbitals; on the contrary, the ferromagnetic coupling can be formed by 180° exchange between filled and empty cation orbitals or 90° exchange between filled cation orbitals.

b) Double-exchange

Compared to super exchange, which is based on a virtual hopping mechanism, double-exchange is a real hopping process. In other words, the electrons in super exchange are localized, but they are delocalized in double-exchange interaction. Double-exchange often happens between ions in different oxidation states. Furthermore, the electron hopping process is accompanied by ferromagnetic alignment of the metal atoms.

c) Interaction in Fe_3O_4

As shown in Figure 2.2, the dominating interactions are mainly three:

1. Antiferromagnetic coupling between the T_d and O_h cations, induced by the superexchange interaction with an angle in between of 125° as shown in Figure 2.2(a).

2. Ferromagnetic coupling between cations on the O_h sites, induced by superexchange interaction with an angle of 92.3° between Fe^{2+}-O-Fe^{3+} as shown in Figure 2.2(b).

3. Ferromagnetic coupling between cations on the O_h sites, driven by double-exchange interaction as shown in Figure 2.2(c).

d) Net magnetic spin in Fe_3O_4

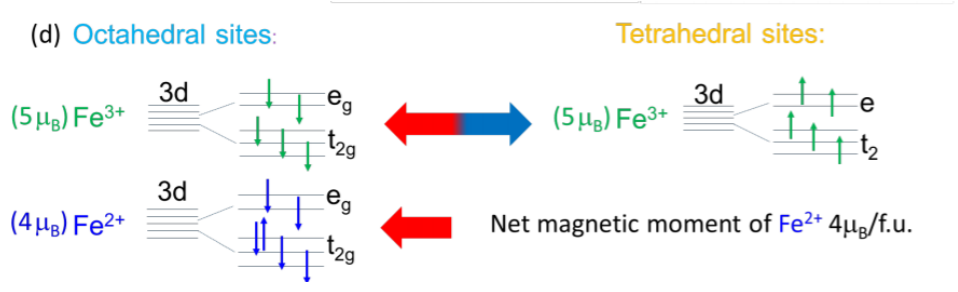

Figure 2.3 Sketch of electron state in Fe_3O_4 (figure taken from ref.[8])

As there is antiferromagnetic coupling between the Fe^{3+} on T_d and O_h sites which is the superexchange interaction, the spin of Fe^{3+} in O_h and T_d can compensate each other as shown in Figure 2.3. As a result, the net magnetic moment is only caused by Fe^{2+}, and is equal to 4μB/f.u.

2.1.3 Verwey transition

The Verwey transition is a first order metal-insulator transition unique to magnetite. It occurs around 120 K[12]. With warming through Verwey transition temperature (T_V), the magnetite crystal lattice changes from a monoclinic structure to a cubic inverse spinel structure. Conducting behavior changes from insulating to metallic.

Magnetocrystalline anisotropy is an intrinsic property of Fe_3O_4, independent of grain size and shape. Depending on different orientation of the sample, the magnetization reaches saturation in different fields. For Magnetite above the Verwey transition temperature, <111> is the easy direction of magnetization and <100> is the hard direction of magnetization. Thus, the magnetization will be saturated in the <111> direction. However, when temperature is lower than Verwey transition temperature, with the changing crystal structure, the easy axis changes to <100> direction. Magnetocrystalline anisotropy is the energy needed to deflect the magnetic moment in a single crystal from the easy to the hard direction.

The change of crystal structure induces the changes in electric and other properties. The first observed change is the metal-insulator transition: when T>120K, electrons can hop from Fe^{2+} to Fe^{3+} and causes conductivity; when T<120K, the electron hopping freezes out and the resistivity increases enormously. Verwey transition is an important property of Fe_3O_4. Some research has studied the dependence of the Verwey transition on the oxygen content[13]. With increasing oxygen content, Fe_3O_4 changes from the first-order phase transition to second-order transition and the discontinuity will finally disappear. As shown in Figure 2.4, for $Fe_{3-\sigma}O_4$, with increasing nonstoichiometric σ, the Verwey transition temperature decreases[14]. Thus, it is a good indicator of stoichiometry.

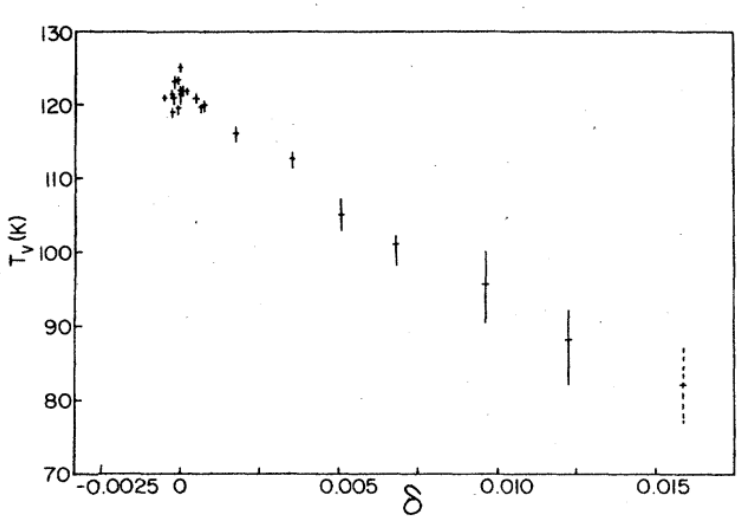

Figure 2.4 Verwey transition temperature verses nonstoichiometric parameter σ (figure taken from ref.[14])

2.2 Yttria-stabilized zirconia (YSZ) substrates

During deposition oxide substrates can reduce or oxidize the Fe_3O_4 thin films. In this study, we want to optimize the growth parameters and study the influence of different growth parameters. Different substrates have different oxygen supply characters. For example, Strontium titanate can oxidize Fe_3O_4 and supply oxygen to the thin films which complicates the growth parameters optimization[15]. Thus, we choose yttria-stabilized zirconia (YSZ) as oxide substrate, which has "inert" oxygen supplying properties. In other words, YSZ as a substrate doesn't supply oxygen to Fe_3O_4 thin film. This makes YSZ ideal for the optimization of growth parameters.

2.2.1 YSZ crystal structure

The main phase of YSZ is ZrO_2, which is monoclinic at room temperature and unstable cubic at 2370 °C. It is stabilized by doping with Y_2O_3 to reach a stable cubic structure at room temperature. YSZ is an insulator with a face centered cubic structure and a lattice constant of 5.16Å.

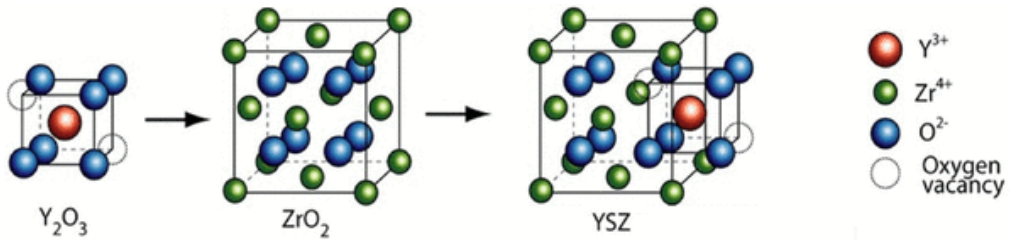

Figure 2.5 Crystal structure of YSZ (figure taken from ref.[16])

2.2.2 Epitaxial growth of Fe_3O_4 on YSZ substrates

The lattice constants of Fe_3O_4 and YSZ are 8.395 Å and 5.16Å, respectively. The lattice mismatch between Fe_3O_4 (100) and YSZ (100) is larger than 30%. This high mismatch forces Fe_3O_4 film to grow parallel to the (111) planes. The new mismatch between the Fe_3O_4 (111) and YSZ (100) is 6%, which is acceptable for heteroepitaxial film growth[8].

2.2.3 Gibbs free energy

Different oxide substrates can influence the reduction and oxidation at the interface between Fe_3O_4 and substrates[17]. The direction of reduction and oxidation reaction can be determined by the Gibbs free energy. As from thermodynamic definition, a reduction in Gibbs free energy is necessary for a reaction to be spontaneous at constant pressure and temperature. This means when the Gibbs free energy of oxide substrate is lower than Fe_3O_4, such as the Gibbs free energy of STO ($\Delta G^0_{STO} = -1500 kJ/mol$) is lower than Fe_3O_4 ($\Delta G^0_{Fe_3O_4} = -1164.21 kJ/mol$), then the STO substrate can reduce Fe_3O_4 thin film and results in a more complicated system[15]. However, the Gibbs free energy of YSZ ($\Delta G^0_{YSZ} = -1200 kJ/mol$) is similar to Fe_3O_4, which is ideal for the optimization of growth temperature.

3 Experimental methods and instruments

This study aims to find the appropriate deposition temperature, laser size and laser energy for Fe_3O_4 deposited on YSZ substrates. The instruments used for preparation and characterization of the sample are introduced in this chapter. Pulsed laser deposition (PLD) is used to prepare the sample. The X-ray reflectometer and atomic force microscope provide the information of surface roughness and structure of the film.

3.1 Pulsed laser deposition (PLD)

Pulsed laser deposition (PLD) is a physical vapor deposition (PVD) technique which is often used to deposit thin films on substrates. In a vacuum chamber, a high-power pulsed laser beam is focused on a Fe_2O_3 target and therefore, the target material is deposited. The vaporized target material deposits as a thin film on the substrates. This deposition occurs in the presence of a background gas – oxygen, which is commonly used when depositing oxides to fully oxygenate the deposited films. The deposition parameters influence the quality of the crystallization of thin films.

The PLD process involved can be described as below: a 50W KrF excimer laser with a pulse width of 25ns and a wavelength of λ=248nm is used. As shown in Figure 3.1, the high-power laser pulse is focused in a vacuum chamber on the rotating target. The material of the target (here Fe_2O_3) is vaporized to form a plasma plume. The ablated material consists of the neutral and ionized species, and then this material is directed to a substrate, which is 50 mm away from the target. The laser fluence F, which is calculated by the energy of laser pulses and the size of the laser spot on the target, is important for the ablation process. The laser fluence and the pulse repetition rate can be adjusted between $F = 1-3$ J/cm^2 and $f = 1 - 50$ Hz, respectively.

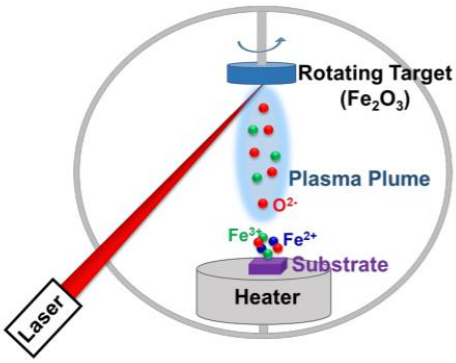

Figure 3.1 Sketch of PLD process (figure taken from ref.[8])

The film does not necessarily have the same composition as the target, in order to deposit Fe_3O_4 thin films, we choose the stable phase Fe_2O_3 as target material. By changing the background oxygen pressure, desired film stoichiometry can be reached. In this study, the base oxygen pressure is $1x10^{-7}$ mbar. In addition, the substrate is mounted on a heater which can reach maximum 850°C. By controlling the heat, sufficient energy can be introduced for adatoms to diffuse and arrange themselves to form the desired crystalline structure

3.2 Atomic force microscopy (AFM)

The Atomic Force Microscope Agilent 5400 is used here to characterize the surface morphology of the films and substrates with a sub nanometer resolution. By measuring the interaction force between the tip and the sample, an image of the topography of a sample surface at a high resolution can be easily made.

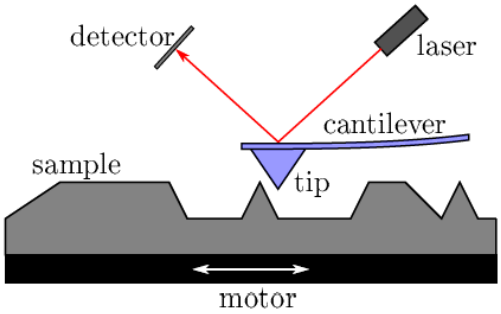

Figure 3.2 Principle of AFM measurement (figure taken from ref.[18])

As shown in Figure 3.2, the laser is reflected by the cantilever to the detector. Tapping mode is the most common mode of AFM. In tapping mode, the cantilever is driven to oscillate near its resonant frequency, which is achieved with a piezo element in cantilever holder. The frequency and amplitude of the driven signal are kept constant. When the tip is close enough to the sample surface interaction forces affect the amplitude of cantilever oscillation. Through a feedback system, the height of cantilever is adjusted, and thus the surface topography mapped.

3.3 X-Ray Reflectometry/ Diffractometry (XRR and XRD)

X-Ray Reflectometry is a sensitive tool to characterize the surface of a thin film, here two devices are used: Bruker D8 Advance from JCNS-2 and Bruker D8 Advance from PGI-7 (thanks to Prof. Dittmann). They share the same principle but have different resolutions and options. Cu-source is used as X-ray source with a wavelength $\lambda = 1.54\text{Å}$ in both instruments.

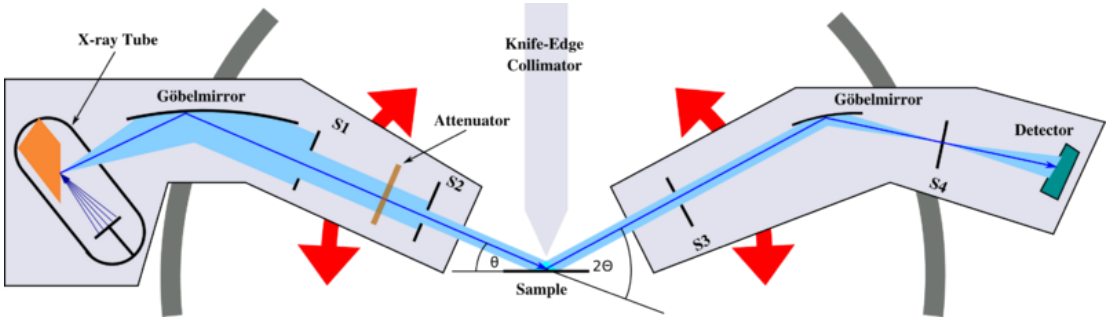

Figure 3.3 Sketch of D8 XRR (figure taken from ref.[19])

As shown in Figure 3.3, the X-Ray goes through slits and are reflected by a smooth sample to the detector. By analyzing the intensity of reflected X-Ray, we can get information of thickness and roughness of the thin film.

At the surface of thin film samples, both reflection and refraction of X-Ray occur as shown in Figure 3.4.

The relation between incident and refracted X-Ray beam is:

$$n_1 \cos(\alpha_i) = n_2 \cos(\alpha') \qquad (2-1)$$

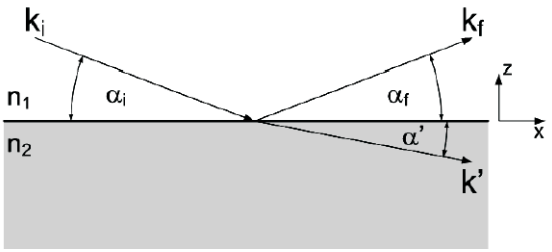

Figure 3.4 Reflection and refraction of x-ray (figure taken from ref.[20])

The index of most materials is smaller than one, the index of air is equal to one. As a result, when we consider an X-Ray beam incident from air and refracted in thin film, then there would be a critical angle α_c for the incident beam. When the incident angle α_i is smaller than α_c there is no refraction, which is called "total internal reflection". For a Fe_3O_4 thin film, α_c = 0.2 °.

For a single thin film system, the refracted beam will be reflected at the interface between substrate and thin film, then constructive interference occurs with the reflected beam at the surface of the thin film, as shown in Figure 3.5. This phenomenon causes the oscillation pattern with angle which is called "Kiessig fringes". By analyzing the period of these oscillations, thin film layer thickness and interlayer roughness can be calculated.

X-ray reflectivity measurement are often analyzed by fitting the measured data to a simulated curve. Fitting parameters are layer thickness, densities, roughness. Here, the program GenX[21] is used for analysis.

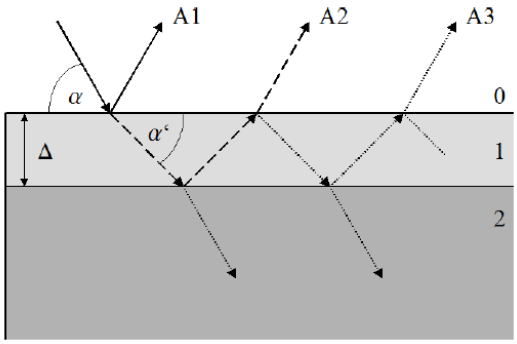

Figure 3.5 Constructive interference in single thin film system (figure taken from ref.[20])

X-Ray diffractometry experiment is also an ideal tool to characterize crystal structure of thin film layer. Based on Bragg's law (formula 2-2), incident X-ray shows an interference pattern after interaction with lattice. Lattice constant d is easily calculated.

$$2d\sin\theta = n\lambda \qquad (2-2)$$

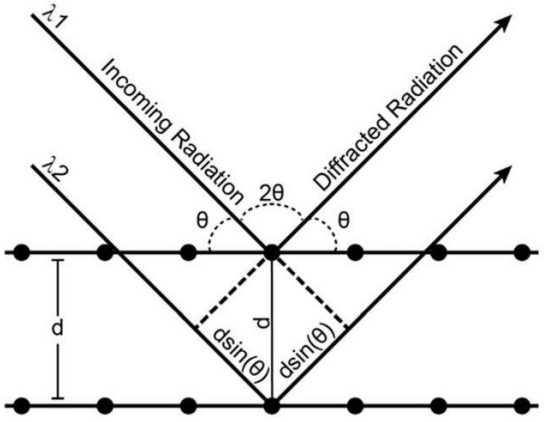

Figure 3.6 Bragg's law (figure taken from ref.[22])

n: A whole number

λ: Wavelength of X-ray which is 1.54 Å in our device

d: distance between two layers

θ: reflected angle

The Laue oscillation happens when the Laue equations fulfilled. Laue equations relate incoming waves to outgoing waves in the process of elastic scattering by a crystal lattice[23]. These Laue oscillations, due to the finite thickness of the film diffracting the incoming beam, are indicative of films smooth interfaces and very high crystalline films quality. From Laue oscillations the film thicknesses t can be determined with Formula 2-3, where λ is the wavelength of the x-rays , θ_{i+1} and θ_i are two adjacent maxima in the oscillations[24]. With this formula we can calculate the thickness of crystalline part in thin films.

$$t = \frac{\lambda}{2(\sin\theta_{i+1} - sin\theta_i)} \qquad (2-3)$$

3.4 Vibrating sample magnetometer (VSM)

The PPMS DynaCool from Quantum Design is used here[25]. In DynaCool, a single two-stage Pulse Tube cooler is used to cool the system, providing a continuous low temperature control (1.9K to 400K) and precise field (magnetic field up to $\pm$9T) and temperature sweep modes.

By using vibrating sample magnetometer (VSM) mode, the influence of environment can be minimized and the magnetic properties of samples measured. First a sample is magnetized in a uniform magnetic field and then sinusoidally vibrated. The magnetic field is generated by a superconducting solenoid which has a vertical field, meaning it aligns with <100> axis of sample.

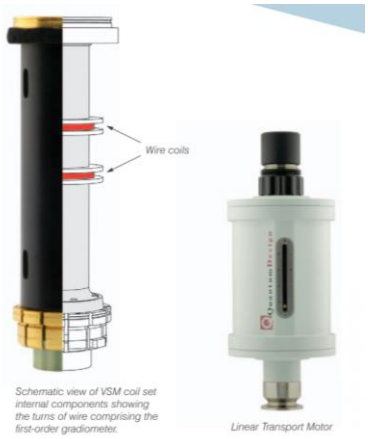

Figure 3.7 VSM coil set and linear transporter (figure taken from ref.[25])

By using VSM, the magnetic moment of substrate and thin film can both be measured. By subtraction of the diamagnetic part of substrate, the magnetic moment of the Fe_3O_4 thin film can be extracted.

3.5 Physical property measurement system (PPMS)

Physical Property Measurement System (PPMS) from Quantum Design is used to measure the electric properties of thin film system.

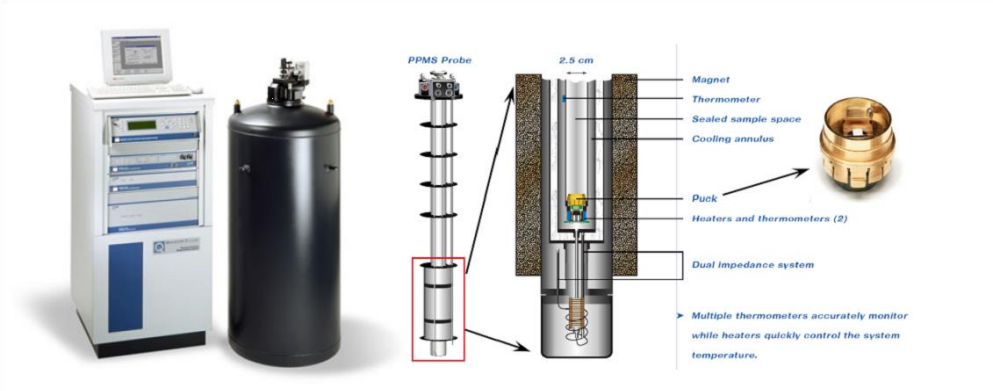

Figure 3.8 Sketch of PPMS measurement system (figures taken from ref.[25])

Figure 3.8 shows the sketch of PPMS measurement system. In order to measure the resistance, the Van-der-Pauw method is used when bonding the sample on the puck. Van-der-Pauw method is commonly used to measure the resistivity of a thin film which should be homogenous and isotropic with a uniform thickness. The Van-der-Pauw method adopts a four-point contacts in the four edges of samples with puck, this four-point contacts should be much smaller than the thin film area. Compared with linear four-point probe, Van-der Pauw method can provide an average resistance of the whole sample, instead of only in the sensing direction. In our case, in order to connect thin film sample with the puck, we are using the wedge bonder from Kulicke & Soffa (Model 4523D) with AlSi (1%) wire. Compared to bonding the sample with platinum wire and silver paint, the wedge bonder allows us to reach a much smaller connection and also avoid silver paint, which could possibly diffuse inside the thin film and cause additional conductance.

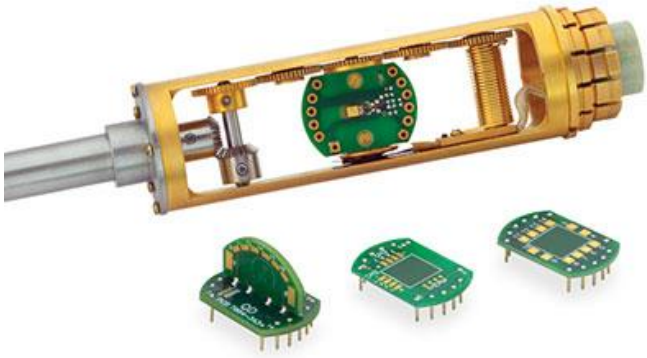

Figure 3.9 Horizontal rotator and its pucks (figure taken from ref.[25])

Figure 3.9 shows the puck of horizontal rotator, which allows the measurement of samples at different angle (especially 90° and 180°)

4. Structural and physical properties of Fe_3O_4 thin films in relationship to different growth parameters

The samples of Fe_3O_4 thin films on YSZ substrates are grown by pulsed laser deposition (PLD). As there is a huge lattice mismatch between Fe_3O_4 thin films and YSZ substrates, it is important to find appropriate growth parameters for a relaxed film lattice. Among all the growth parameters of the deposition process, the most important one is the growth temperature which will be discussed in detail in section 4.3 – 4.5.

4.1 Sample preparation

The 5mmx5mmx0.5mm YSZ substrates from Crystec GmbH are annealed at 1100°C for 8 hours in order to achieve the better surface quality of the substrates. The different AFM images before and after annealing are shown in Figure 4.1. After annealing, the morphology changes to a terraced structure which indicates a better crystallinity.

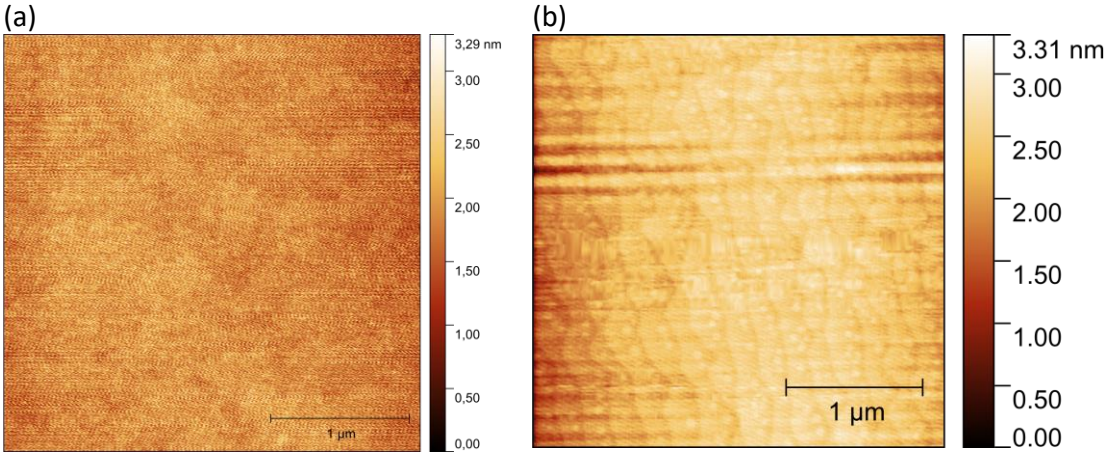

Figure 4.1 AFM images of YSZ substrates (a) before annealing and (b) after annealing at 1100°C for 8h

The substrate is always considered as the main parameter for thin film growth. As mentioned in section 2.2, the huge lattice mismatch lattice between Fe_3O_4(100) and YSZ (100) forces Fe_3O_4 film to grow parallel to (111) plane. In order to get epitaxial films, a lattice mismatch less than 7%-9% is required. The new mismatch of 6% between Fe_3O_4(111) and YSZ (100) allows magnetite to grow epitaxially.

4.2 Laser fluence

Fe_3O_4 thin films are prepared by PLD. The Fe_2O_3 target is from Praxair with purity of 99%. After placing the substrates inside the chamber, the chamber is pumped up to reach a high vacuum condition which is ca. 2 x 10^{-6} mbar.

Before starting the deposition, we clean the target and the substrate. First, we anneal the substrate at 500°C for 90 min in order to clean the substrate of contaminants, and then we set the laser energy to 10kJ for 30 sec. to clean the target and get high quality films.

During the deposition, some parameters are fixed as mentioned in chapter 3.1. The growth parameters are essential to understand as they influence the quality of thin films. Here we set different laser fluence and substrate temperature in order to study their influence on the properties of Fe_3O_4 thin films.

Laser fluence is calculated by the formula 4-1:

$$\text{Fluence}\left(\frac{\text{Joules}}{cm^2}\right) = \frac{Laser\ pulse\ energy\ (J)}{Effective\ focal\ spot\ area\ (cm^2)} \qquad (4-1)$$

We observed different morphology in AFM images shown in Figure 4.2. Figure 4.2(a) shows a bright spot in the middle, with the increasing of laser fluence from 1.62 to 3.47 J/cm^2, this island-mode growth becomes less and the surface becomes more homogeneous. At the same time, the maximum height difference of thin films decreases from 85nm to 13.6nm which indicates a good film quality at 3.47J/cm^2.

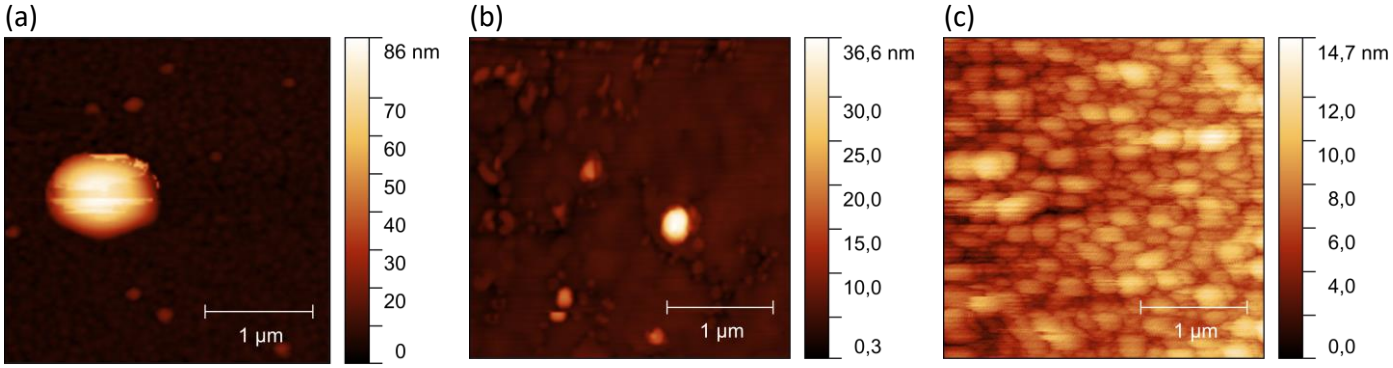

Figure 4.2 AFM images of Fe_3O_4 thin films grown on YSZ substrates at laser fluence of (a) 1.62J/cm^2 (b) 2.08J/cm^2 and (c) 3.47J/cm^2

XRR results are shown in Figure 4.3(a). There is not a big decrease of initial intensity which is associated with the roughness of thin films. The curves are fitted by GenX[21] software and

roughness is plotted in Figure 4.3(b). The roughness is around 0.7nm and doesn't change much for different fluence. However, as shown in Figure 4.3(c), the film thickness changes a lot with laser fluence. As discussed in the study done by M.H. Hamed, the film thickness influences the quality of films[26]. When the film is too thin, the interface properties dominate, however, with thickness more than 38nm, we observe a more bulk-like behavior. With a fluence of 3.47J/cm^2, we get a smooth surface from AFM and the quality of crystallinity need to be checked.

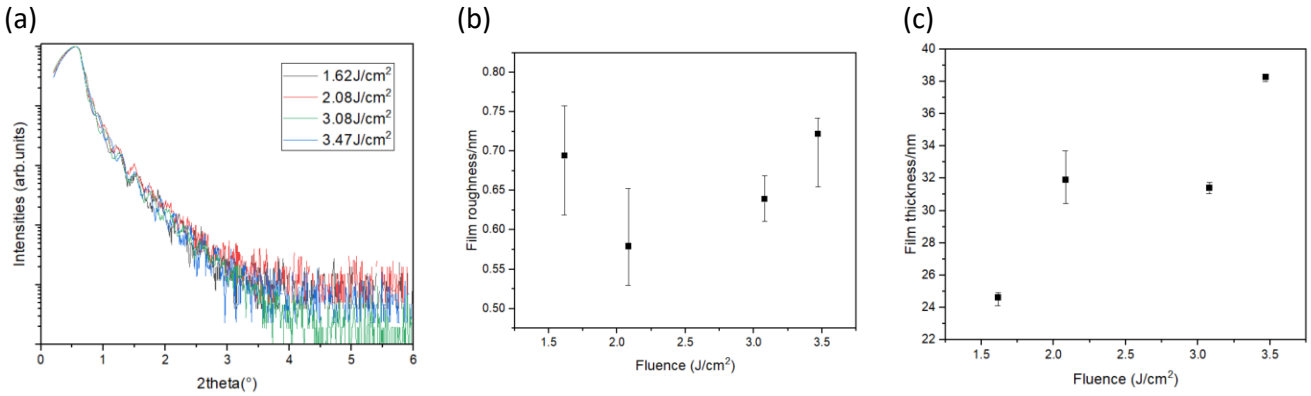

Figure 4.3 (a)XRR results of Fe_3O_4 thin films grown on YSZ substrates at different laser fluence and the (b) roughness, (c) thickness calculated from XRR results with the deposition time of 25min.

By checking the XRD results as shown in Figure 4.4(a), there are only Fe_3O_4 peaks along (111) direction which indicates the single crystallinity in out-of-plane direction. It's clear that for the smaller laser fluence, the peak of magnetite is very weak, but for the larger laser fluence, the film peaks become clearer and strong. If we zoom in the two-theta value between 30 and 41° as shown in Figure 4.4(b), for lower fluency there are additional peaks of α-Fe_2O_3(006) around 39.24°; with higher laser fluency, there are only peaks of Fe_3O_4. The peaks around 23° could be the reflection of α-Fe_2O_3 which we will investigate in my further master thesis. Besides, we can also see the clear Laue oscillation for the larger laser fluence.

Thus, we chose the laser fluence of 3.47 J/cm^2 and make a temperature series from 400 to 600°C in the further measurement.

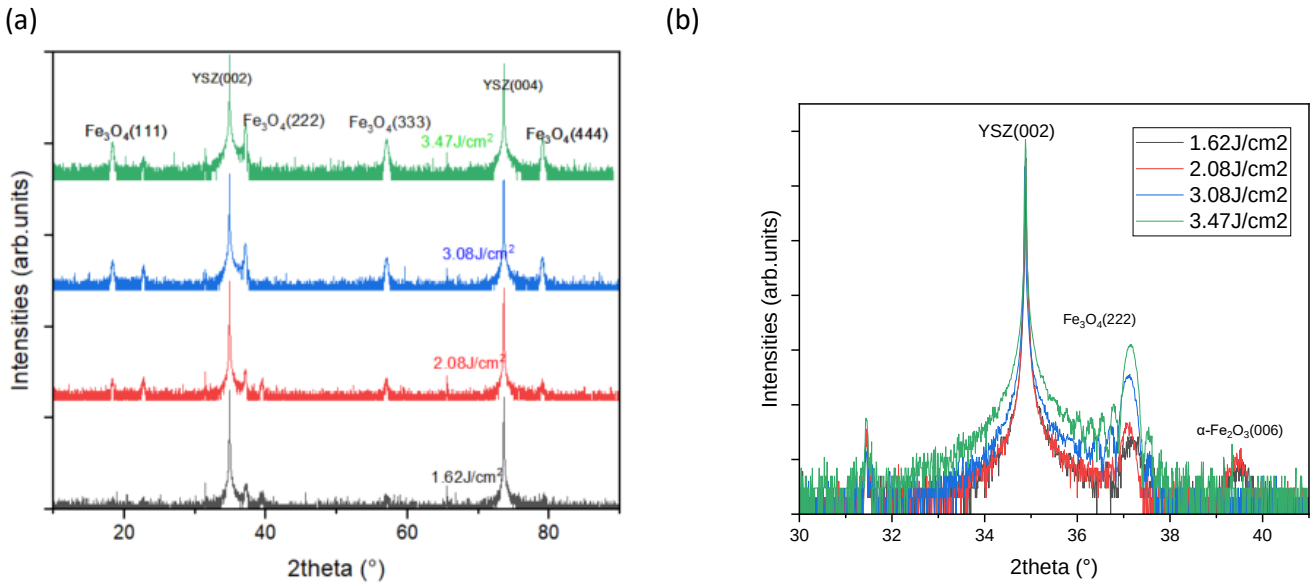

Figure 4.4 XRD results of Fe_3O_4 thin films grown on YSZ substrates at different laser fluence with two theta value of (a) 10-90° and (b) 30-41°.

4.3 Morphological and structural dependence on substrate temperature

The growth temperature is important for the crystal structure of the film, which will influence the physical properties of the film. By changing the growth parameters, we can tune the crystal quality, thickness and roughness of the film, magnetic and electric properties of the film.

Because of the large misfit when Fe_3O_4 growing on YSZ substrates, the large surface roughness is challenging for deposition. The surface morphology, roughness and thickness can be characterized by atomic force microscopy (AFM) and X-ray reflectivity (XRR). By using XRD, the crystal structure can be analyzed.

4.3.1 AFM

The measurements are done in tapping mode in air by Atomic Force Microscope Agilent 5400. The scan size is a square of 5μm x 5μm.

AFM 5μm x 5 μm 2D scans of Fe_3O_4 films grown at different temperature of T_{growth}=400, 450, 500, 550, 600°C are displayed in Figure 4.5. Comparing the YSZ substrate as shown in Figure 4.5(a), the terrace structure of the substrate disappears for all growth temperatures. For the Fe_3O_4 films grown over 500°C, Figure 4.5(e), (f) show the absence of step structure of the YSZ

substrates. This means that during the deposition the thin film doesn't adopt the structure of the substrates surface. Instead of growing layer by layer, the undesired island growth is formed during growth on the substrates.

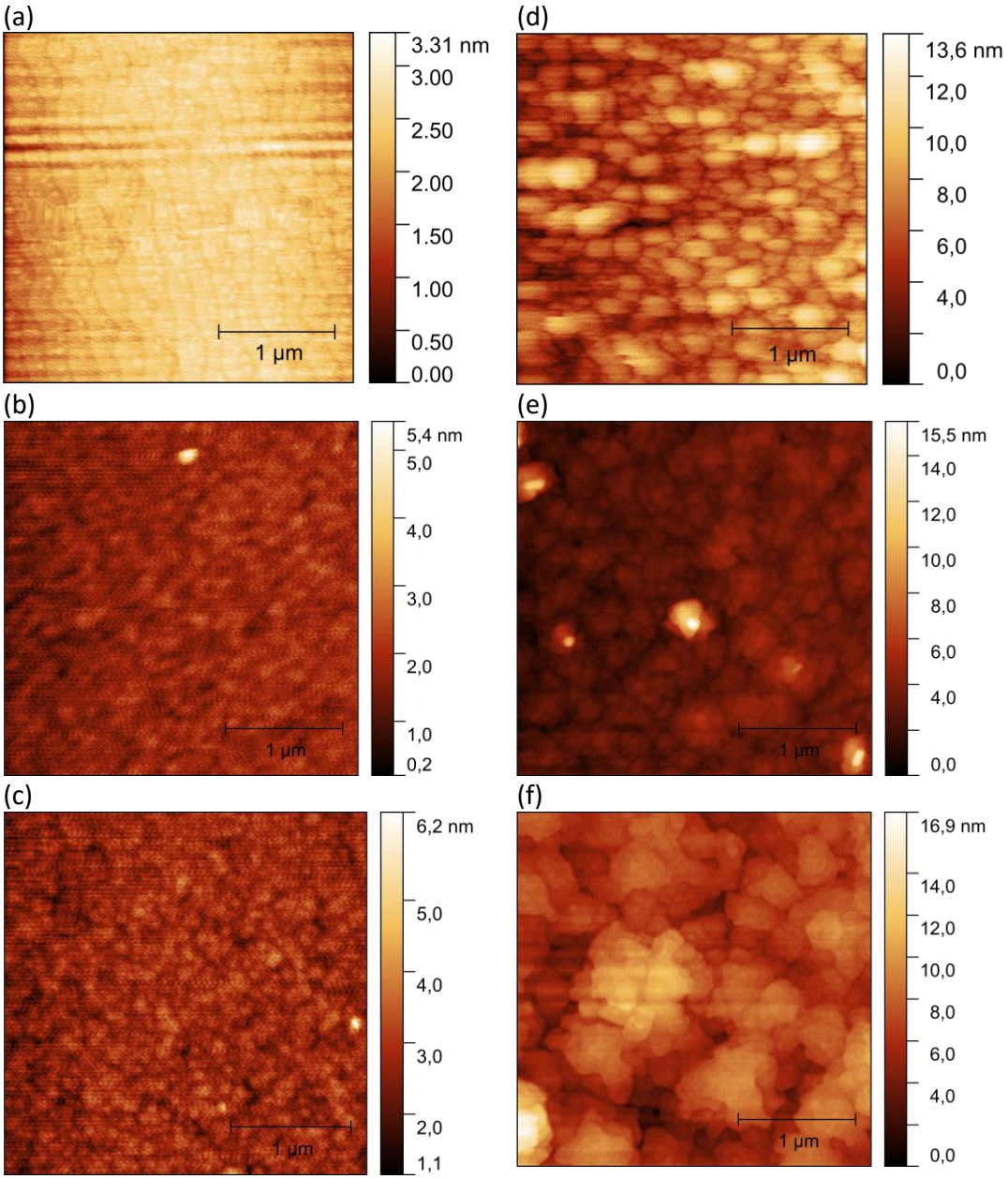

Figure 4.5 2D images of (a) YSZ substrate and Fe_3O_4 thin films grown at a temperature series (b)400°C, (c)450°C, (d)500°C, (e)550°C, (f)600°C.

The surface roughness can be furthermore analyzed by Root Mean Square (σ_{RMS}), analyzed by Gwyddion[27] software. The surface roughness is 0.031, 0.069, 0.082, 0.110, 0.121 nm for the thin films grown at 400, 450, 500, 550, 600°C respectively. The roughness increases strongly with

the increasing growth temperature, also indicating the loss of layer-by-layer structure during growing. Thus, when T_{growth}=400, 450, 500, 550°C, we can make good quality of thin films with small roughness.

4.3.2 XRR

X-ray reflectivity (XRR) is used in our study to investigate the surface roughness and thickness of the thin film by using Bruker D8 Advance.

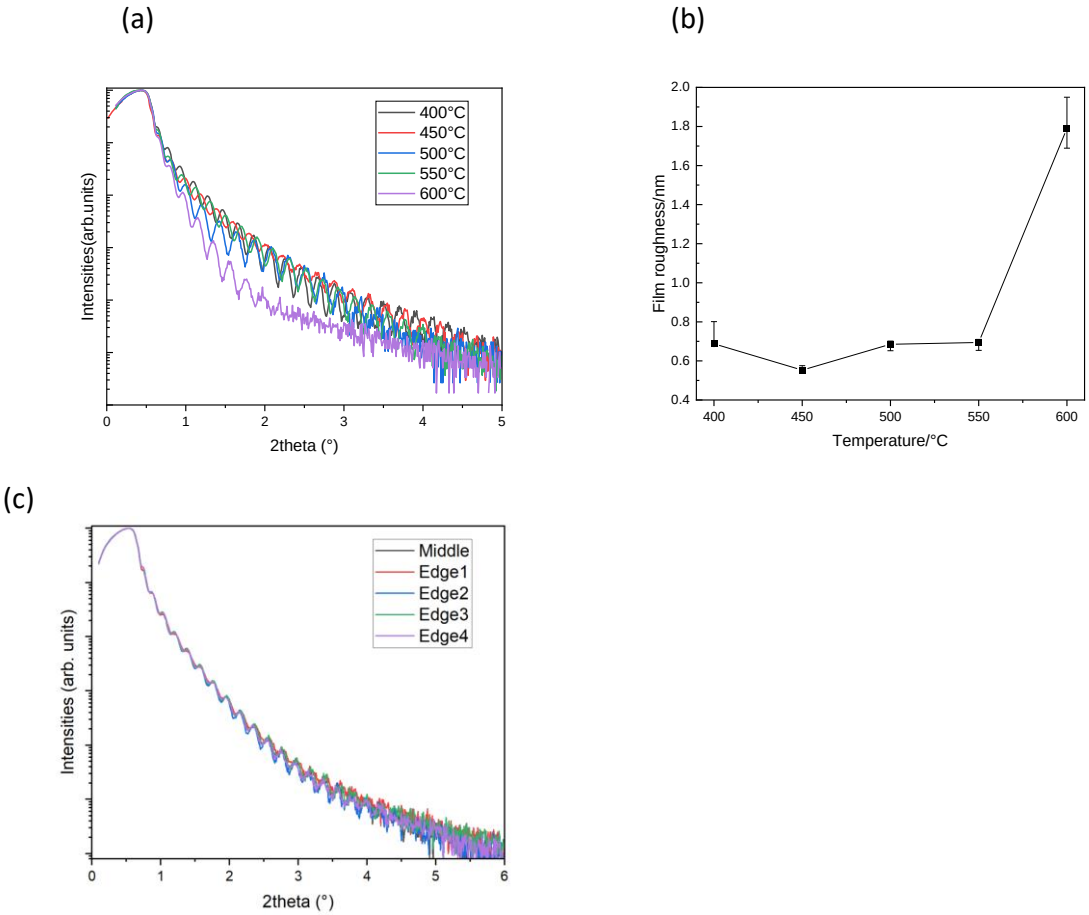

Figure 4.6 (a) X-ray reflectivity of samples grown at different temperatures, (b)surface roughness of films calculated from XRR, (c) XRR for the different position on same sample grown at 550°C.

For incident angles below the critical angle (0.4°), we have total external reflection. Above the critical angle, the roughness of the thin films causes the exponential intensity reduction of the reflected wave. In other words, the intensity drops faster with increasing roughness.

Besides of the roughness of the thin film surface, the thickness can also be concluded. Interference occurs between X-ray inflected from the surface of the thin films and the refracted

part of X-ray reflected from the interface. This interference causes oscillations of the reflectivity. These oscillations were found by Kiessing and named as Kiessing fringes[28]. By analyzing the period of the oscillations, we can calculate the film thickness. The thicker the film is, the shorter the period of the oscillations.

Figure 4.6(a) shows the X-ray reflectivity of Fe_3O_4 thin films at different growth temperature in the range of 2θ=0.1°-6°. The sample grown at 600°C shows a much faster drop after the critical angle compared to the others, which indicates a higher roughness. The measured reflectivity intensity data is fitted by GenX[21]. The thickness and roughness are found after the fitting. The thickness of all thin films grown under different temperature are all around 40nm. Compared to laser fluency, the substrate temperature doesn't have a strong influence on the film thickness. And the roughness of the films obtained by fitting is shown in figure 4.6(b). Although generally the roughness is much higher than the results obtained in AFM, it shows a similar trend. The thin film grown at 600°C shows a much higher roughness than the others which corresponds to the results from AFM. This increasing of roughness correlates with the high growth temperature. When the temperature is too high, energy is supplied for an atom to diffuse and form the island-like structure which contributes to the roughness.

As shown in Figure 4.6(d), XRR measurements are done with the same 1cm x 1cm Fe_3O_4 on YSZ sample with different position where laser hits on with the optimized laser fluency of 3.47 J/cm^2. Results from different positions show a good consistency which indicates the homogeneous thin film.

All in all, by analyzing AFM and XRR results, we found the thin films have a good quality when the growth temperature is under 600 °C.

4.3.3 XRD

After confirmation with AFM and XRR results, we use X-ray diffraction (XRD) to analyze the out-of-plane crystallinity of the thin films by using the device of Brucker-D8. Figure 4.7 (a) shows the XRD scan of Fe_3O_4/YSZ system with the 2θ range from 10° to 90°. The results are normalized to YSZ (002) reflection. The peaks of substrates, YSZ (002) and YSZ (004) reflection, are strong and clear, which helps to align the beam. The peak around 31.5° is caused by Cu K_β. Using formula 2-2, the 2theta value of YSZ (002) is associated not only with the

lattice constant but also the wavelength of the X-ray source. For Cu K_α, the wavelength is 1.54 Å, which causes the strongest peak around 34.9°, while the wavelength of Cu K_β is 1.39 Å and causes the peak around 31.5°. Between, the four peaks of Fe_3O_4 in (111) direction all show up, while the other character peaks of Fe_3O_4 do not. This indicates the Fe_3O_4 crystals are grown in the same direction. In another word, films at all temperature are grown in layer by layer mode with single crystallinities.

In order to investigate the local behavior, figure 4.7(b) shows the XRD scan with the 2θ ranged from 30° to 40° around the YSZ (002) and Fe_3O_4 (222) reflection. First of all, there are clear Laue oscillations for the films grown at all the different temperatures which indicates the good quality of the films. From XRR and Laue oscillation, the thickness of thin films can be calculated. As shown in Figure 4.7(c), the thickness of thin films grown at different temperature calculated from XRR results is around 38nm. As mentioned in section 3.3, Laue oscillation is associated with the crystallinity. Thus, the thickness calculated from Laue oscillation is the thickness of the crystalline part of the film. There could be some dead layers which is amorphous in our thin film system and don't appear in the Laue oscillation. That could be the reason that the red curve is lower than the black one. However, the difference between the thickness of thin films and crystallinity is only around 2 nm, which indicates the good crystallinity of the entire film layer.

The bulk value of the Fe_3O_4 (222) peak is around $2\theta=37.1°$ (blue dashed line). For all the Fe_3O_4 films grown at different temperatures, the Fe_3O_4 (222) peak positions are slightly shifted. The (004) peak occurs at a smaller angle when T_{growth} = 400°C and 450°C, while the same peak occurs at a larger angle when T_{growth} = 500°C, 550°C and 600°C.

As mentioned in section 2.2.2, the bulk lattice constant of Fe_3O_4 crystal in (100) direction at room temperature is 8.395Å, and it is 5.125Å for YSZ in (100) direction. The mismatch is over 30% which drives Fe_3O_4 to arrange in (111) direction where the interplanar spacing now is 5.16Å. Ideally, as shown in figure 4.8 II) the Fe_3O_4 film grows relaxed which means the out-of-plane lattice constant (c_{oop}) and the in-plane lattice constant (a_{ip}) should be equal to the bulk value 5.16Å (c_{oop}= a_{ip} =5.16Å). In contrast, as shown in figure 4.8 III), if the film is totally strained, then the in-plane lattice constant of Fe_3O_4 films should be equal to the in-plane lattice constant of substrate ($a_{substrate}$), which means a_{ip} =$a_{substrate}$ =5.125Å. If we assume the volume of

every lattice would stay constant, then the out-of-plane lattice constant will become larger with the decreasing in-plane lattice constant for the films. Vice versa, as shown in figure 4.8 I), when with tensile strain, the out-of-plane lattice constant will become smaller with increasing in-plane lattice constant.

By using Braggs law given in formula 2-2, the out-of-plane lattice constant can be calculated corresponding to the XRD 2θ value. It is plotted in figure 4.7(d) with changing growth temperature. The region of plots can be divided to three parts, indicating I) tensile strain, II) relaxed growth and III) compressive strain. Generally, the out-of-plane lattice constants of Fe_3O_4 films grown under all temperatures from 400°C to 600°C are all near to the bulk value of 8.395 Å. For T_{growth} = 400°C and 450°C, c_{oop} is only slightly smaller than the bulk value, which means the thin films are grown totally relaxed. However, when T_{growth} = 500°C, 550°C and 600°C, c_{oop} is smaller than the bulk value, indicate the thin films lattice is under tensile strain.

Figure 4.7(e) shows the FWHM (Full width at half maximum) of Fe_3O_4 (222) reflection peaks with different growth temperatures. When T_{growth} = 400°C, FWHM reaches the minimum, which means the best single crystallinity. When T_{growth} = 450°C and 500°C, FWHM is larger. The broader peaks could appear when there are different orientations inside the thin films.

4.3.4 Discussion

We made a series of experiments at different growth temperatures of Fe_3O_4 thin films on YSZ substrates. We have shown that the growth temperature influences the quality of thin films. When T_{growth} < 600°C, the roughness is small while when T_{growth} = 600°C, the surface roughness is much higher. This difference of roughness could be a result of the different growth mode of thin films. When the growth temperature is relatively low, ions of thin films tend to grow epitaxially on the substrates. As these ions adopt the surface structure of substrates, the thin films will be under strain because of the high lattice mismatch between substrate and magnetite (6%). When the growth temperature is relatively high, ions have enough energy to move and rearrange on the YSZ substrates. They would not adapt the epitaxial growth pattern, but instead grow in island mode.

(a)

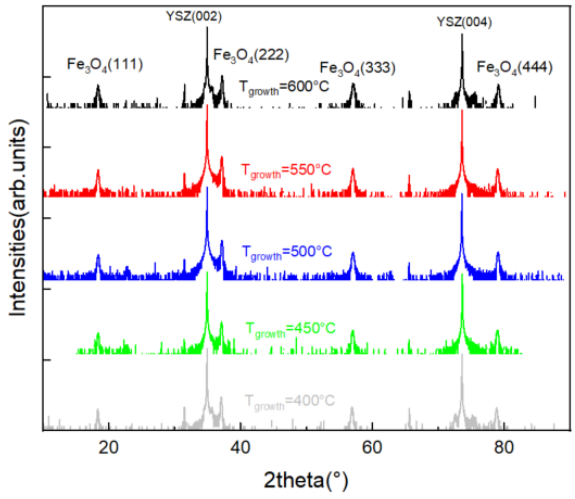
YSZ(002)
YSZ(004)
Fe3O4(111)
Fe3O4(222)
Fe3O4(333)
Fe3O4(444)
Tgrowth=600°C
Tgrowth=550°C
Tgrowth=500°C
Tgrowth=450°C
Tgrowth=400°C
Intensities(arb.units)
2theta(°)

(b)

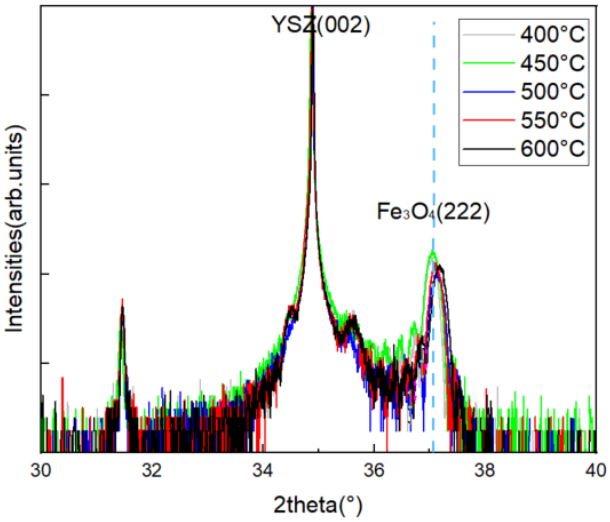
YSZ(002)
Fe3O4(222)
400°C
450°C
500°C
550°C
600°C
Intensities(arb.units)
2theta(°)

(c)

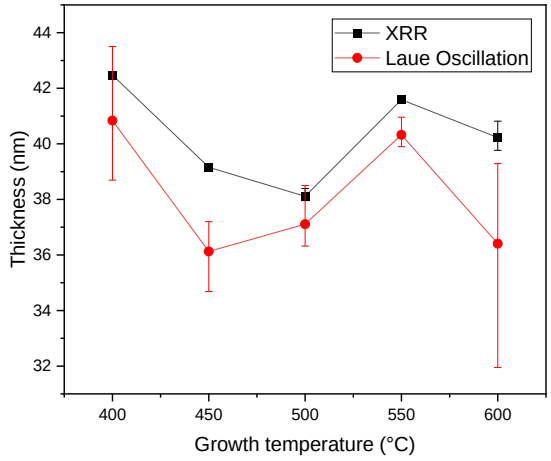
XRR
Laue Oscillation
Thickness (nm)
Growth temperature (°C)

(d)

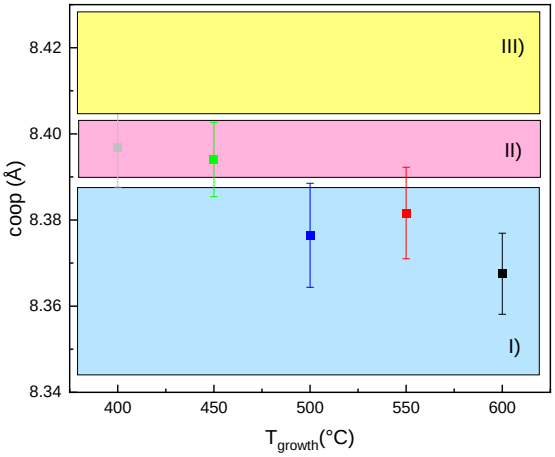
III)
II)
I)
coop (Å)
Tgrowth(°C)

(e)

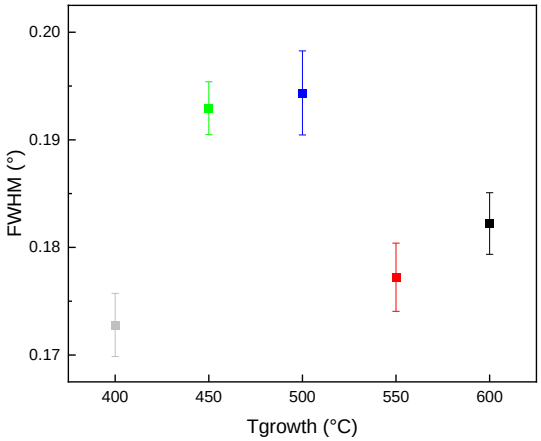
FWHM (°)
Tgrowth (°C)

Figure 4.7: Out-of-plane X-ray diffraction scans of Fe_3O_4 thin films grown at different temperatures of (a) all reflection in the range of 2θ=10°-90° and (b) Fe_3O_4(222) reflection in the range of 2θ=30°-40°. (c) thin films thickness calculated from XRR (black curve) and Laue oscillation (red curve), (d) the out-of-plane lattice constant c_{oop} with different force regions: I) tensile strain, II) relaxed growth and III) compressive strain. (e) Full width at half maximum of Fe_3O_4(222) reflection peaks.

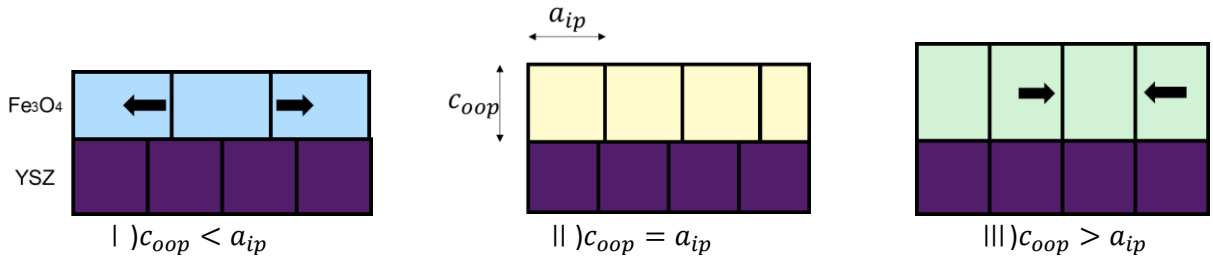

Figure 4.8 Sketches of Fe_3O_4 crystal unit cells on YSZ in different situation: I) tensile strained, II) relaxed, III) compressive strained.

4.4 Magnetic properties

Magnetic properties of Fe_3O_4 thin films at different growth temperatures will be discussed. We are mainly interested in the saturation magnetization, coercivity and Verwey transition temperature.

4.4.1 Experiment details

The vibrating sample magnetometry (VSM) of device PPMS DynaCool (Quantum Design) is used to characterize the magnetic properties of samples. Magnetization versus temperature (M(T)) curves are recorded in zero-field cooling (ZFC) and field-cooling (FC) mode with an applied field of H=500Oe in the direction of YSZ <100>-axis (in-plane). The magnetization versus field hysteresis loops (M(H)) are also recorded at different temperature T=10-300K in the range of H=±2T.

4.4.2 Saturation magnetization

As mentioned in chapter 2.1.1, due to the crystal structure of Fe_3O_4, the spin of Fe^{3+} in O_h and T_d can compensate each other. As a result, the net magnetic moment is only caused by Fe^{2+}, which is $4\mu_B$/f.u. In other words, the theoretical value of magnetite thin films should be $4\mu_B$/f.u.

In order to study on the saturation magnetization of our samples, M(H) behavior has been measured.

The hysteresis M(H) loops are measured by VSM by applying a magnetic field parallel to the in-plane axis <100> of the thin films. As shown in figure 4.9, the Fe_3O_4 thin films grown at different temperatures showed rather different magnetization behaviors. The saturation magnetization for different growth temperatures and measured temperatures is similar around 3 μ_B/f.u.. As mentioned before the theoretical value should be 4 μ_B/f.u., the lower saturation magnetization could originate from the structures while growing. Under different growth temperatures, dislocations and anti-phase boundaries may arise. These kind of anti-phase boundaries are antiferromagnetic, which would contribute to the lower saturation magnetization.

4.4.3 Coercivity and remanence magnetization

Different from the saturation magnetization, coercivity field H_C and remanent magnetization M_r are not constant for different temperatures. Magnetic coercivity is the resistance to changes in magnetization. Coercivity is usually referred to as the magnetic field required to demagnetize the material[29]. As for our Fe_3O_4/YSZ system, magnetite is a ferromagnetic material.

Figure 4.10(a) shows the coercive field for Fe_3O_4 films grown at different growth temperature in dependence of the measurement temperature. With the different tendency, we can divide the graph into two regions to study.

When T > 120K, the coercivities of thin films grown at different temperature shows slight changes, but all remain between 300 – 500Oe. The bulk value of the coercivity of Fe_3O_4 is around 157Oe. This difference could be due to the dislocation and antiphase boundary formed during the deposition of thin films.

When T < 120K, with decreasing temperature, the coercivity increases rapidly. This change is due to the structural transition from cubic to monoclinic at the Verwey transition temperature. Furthermore, Fe_3O_4 thin films grown at different temperatures show different behavior. The samples grown at larger growth temperature shows a stronger increase with the decrease of temperature. This difference could arise from the different strain state with different growth temperature.

(a)

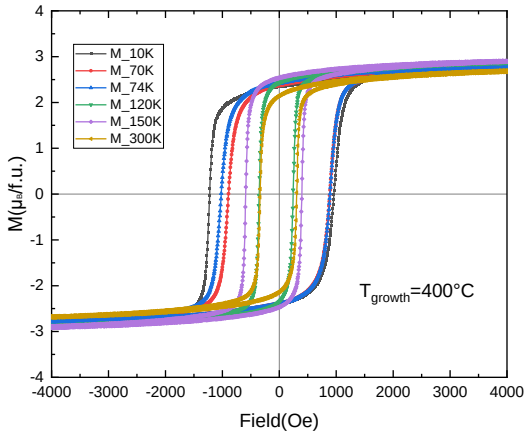
M_10K
M_70K
M_74K
M_120K
M_150K
M_300K
T$_{growth}$=400°C
M(μB/f.u.)
Field(Oe)

(b)

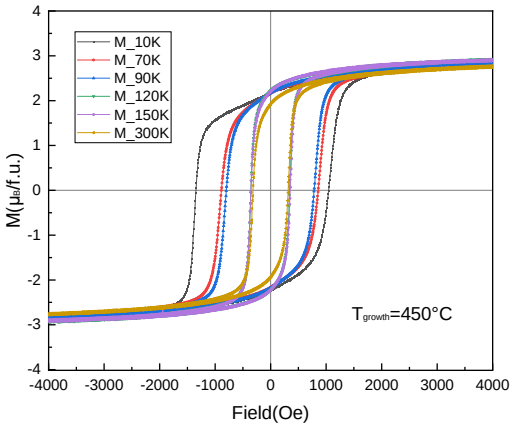
M_10K
M_70K
M_90K
M_120K
M_150K
M_300K
T$_{growth}$=450°C
M(μB/f.u.)
Field(Oe)

(c)

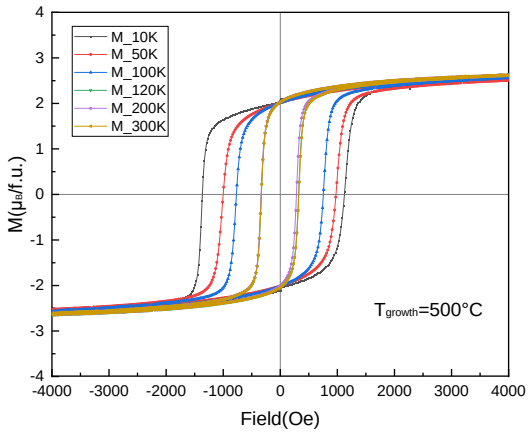
M_10K
M_50K
M_100K
M_120K
M_200K
M_300K
T$_{growth}$=500°C
M(μB/f.u.)
Field(Oe)

(d)

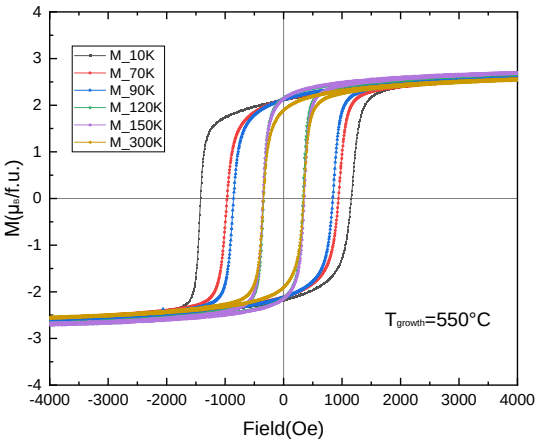
M_10K
M_70K
M_90K
M_120K
M_150K
M_300K
T$_{growth}$=550°C
M(μB/f.u.)
Field(Oe)

(e)

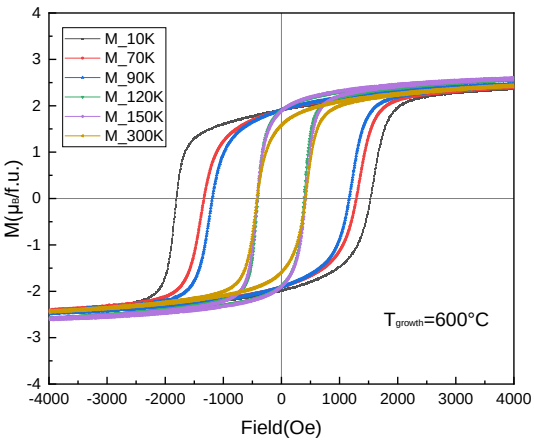
M_10K
M_70K
M_90K
M_120K
M_150K
M_300K
T$_{growth}$=600°C
M(μB/f.u.)
Field(Oe)

Figure 4.9 Hysteresis loop for Fe_3O_4 films on YSZ substrates grown at temperature of (a) 400°, (b) 450°, (c) 500°, (d) 550° and (e) 600 °, measured at different temperatures.

(a) (b)

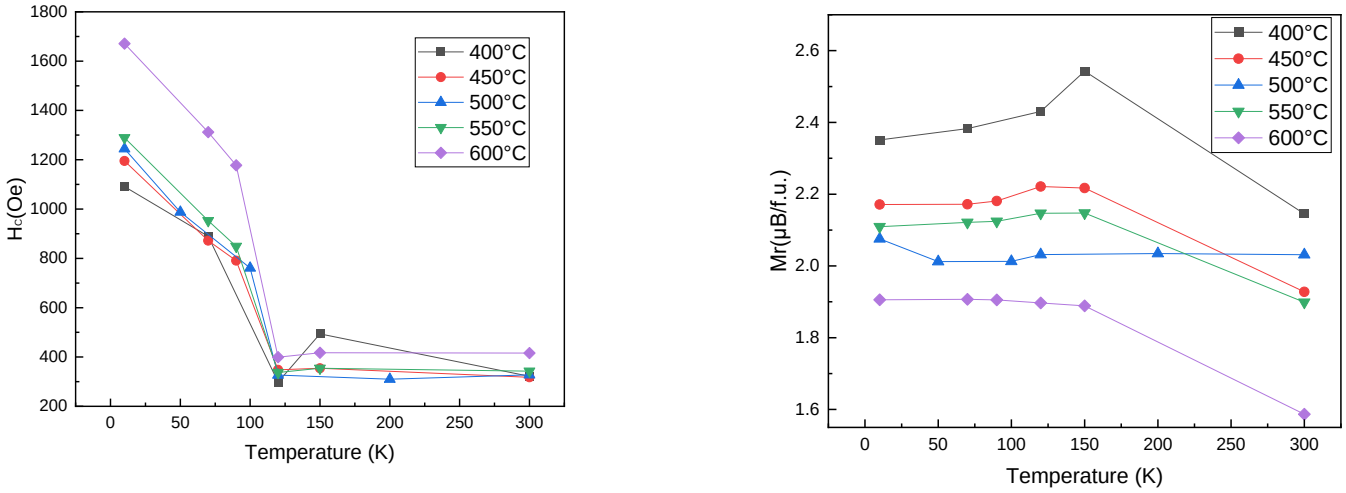

Figure 4.10 (a) Coercive field H_C and (b) remanent magnetization M_r for Fe_3O_4 films grown at different growth temperature and measured at different temperature.

Figure 4.10(b) shows the change of remanent magnetization for Fe_3O_4 films grown at different growth temperature with measurement temperature. For all growth temperature, when temperature is lower than 120K, the remanent magnetization M_r is almost a constant. For most growth temperatures, when T >120K, M_r is decreasing with increasing temperature. It can be explained by the changing of the magnetic easy axis directions. At room temperature, the bulk easy axis is along <111>. When temperature is lower than Verwey transition temperature, the easy axis changes from <110> to <100> with the transformation from cubic to monoclinic. As confirmed by XRD results, there are only peaks of (111) plane in out-of-plane direction. There might be a different growth direction in in-plane, as shown in figure 4.11, which will be investigated in my further master thesis. We also observed the decreasing of remanence with increasing measuring temperature. The increasing temperature can supply the thermal energy and the thermal fluctuations of pinned magnetic moments, therefore, minimizing the effect of anisotropy barriers[30].

All in all, the remanent magnetization and coercivity of Fe_3O_4 thin films grown at different temperature shows the difference of easy axis direction and strain state.

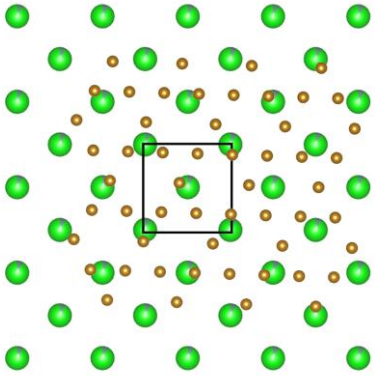

Figure 4.11 Iron atoms of Fe_3O_4 (111) plane (yellow atoms) on Y/Zr atoms of YSZ (001) plane (green atoms)

4.4.4 Verwey transition

The Verwey transition temperature reflects the stoichiometry of the Fe_3O_4 thin films. What's more, because of the structural transition around the Verwey transition temperature, magnetization properties are affected. We should detect a first-order transition around 120K when cooling down the system.

In order to calculate the specific Verwey transition temperature, we measured the change in magnetization with temperature for samples grown at different growth temperatures shown in figure 4.12(a) – (e). The magnetization is measured with zero field cooling and with applying 500Oe magnetic field. The maximal of first derivation $\partial M / \partial \mathrm{T}$ can be use to derive the Verwey transition temperature T_V, the transition width ΔT_V can be derived by the distance between max. and min. of the second derivation $\partial^2 M / \partial T^2$.

As shown in Figure 4.12 (f), all Verwey transition temperatures are below the bulk value which is 124K. The samples grown at 400, 450, 600°C show similar $T_V \approx 115K$, which is nearest to the bulk value.

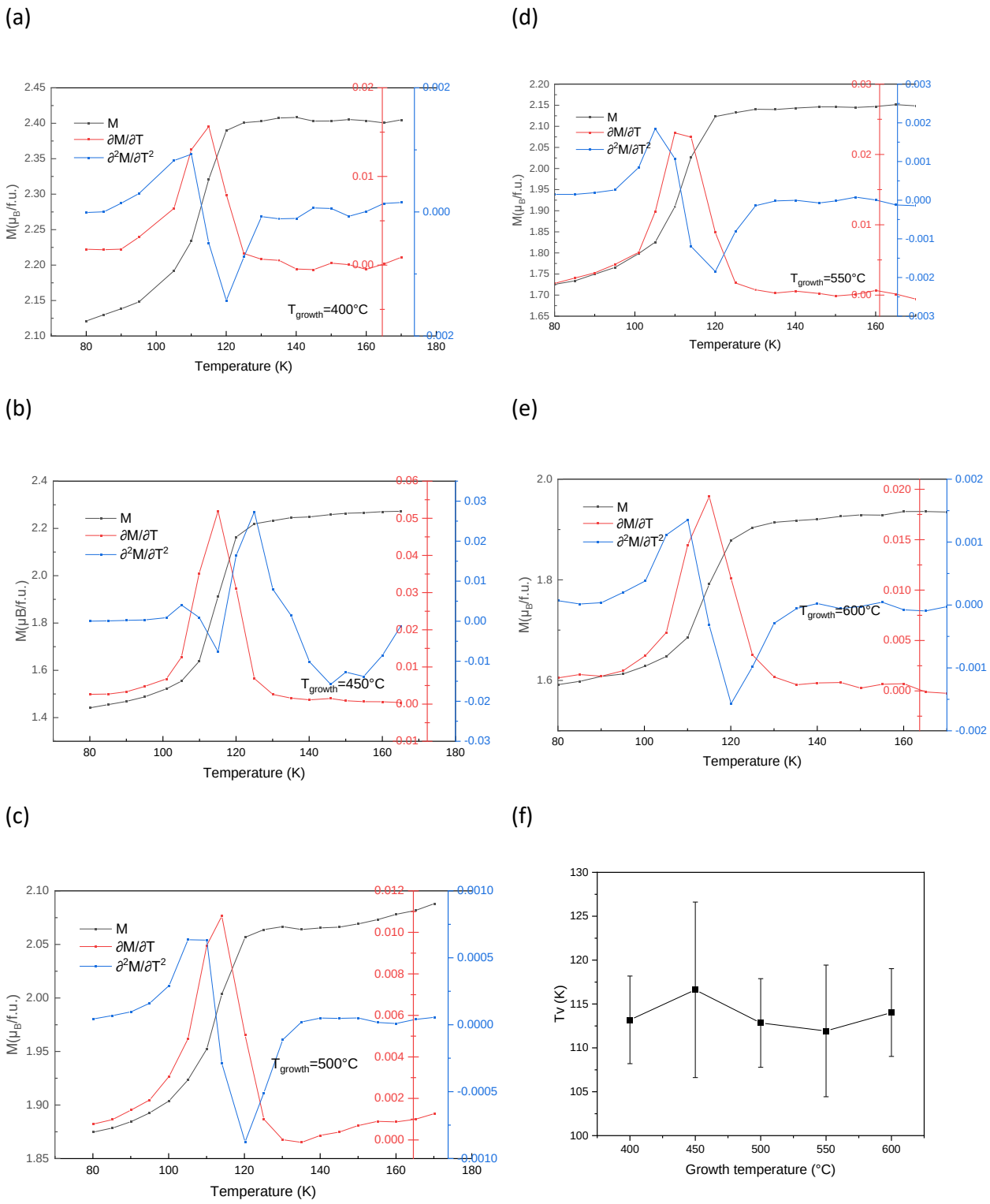

Figure 4.12 Magnetization, first and second derivatives vs. measurement temperature for Fe_3O_4 thin films grown at temperature (a) 400°C, (b) 450°C, (c) 500°C, (d) 550°C, (e) 600°C. (f) Verwey transition temperature vs. growth temperature.

Verwey transition temperature can be influenced mainly by the oxygen stoichiometry, as reported in Barber's' study, for $Fe_{3(1-\delta)}O_4$, when $-0.0005 < \delta < \delta_c = 0.0039$, Verwey transition is still a first-order transition. However, when $\delta_c < \delta < 3\delta_c$ it becomes a second order transition and the discontinuity will disappear[31]. In between, with increasing oxygen content, the Verwey transition temperature will be lower and the width broader. Thus, the generally lower of the trending of the Verwey transition temperature in our experiment could be due to imperfect oxygen stoichiometry.

As the Verwey transition temperature is an indicator of the stoichiometry of Fe_3O_4 thin film, we assume the Fe_3O_4 thin films grown at T_{growth} = 400°C, 500°C and 600°C are either more stoichiometric or more relaxed.

Moreover, as shown in Table 4.1, the transition width is calculated. A systematic study on the influence of stoichiometry on epitaxial Fe_3O_4 thin films discovered that a larger domain size distribution will result in a broader transition[30]. In our experiments Fe_3O_4 thin films grown at T_{growth} = 400°C, 500°C have the sharpest transition which is consistent with the bulk-like Fe_3O_4 thin films.

T_{growth}(°C)	T_V(K)	Magnetization drop (%)
400	113.1919±5	11.8
450	116.6166±10	36.57
500	112.8359±5	10.22
550	111.93±7.5	19.8
600	114.0198±5	17.72

Table 4.1 Magnetization properties of Fe_3O_4 thin films grown at different temperature calculated from M(T) ZFC curve.

Besides of oxygen stoichiometry, strain inside the thin films system can also influence the Verwey transition. As reported in Liu's study, with a relatively high mismatch (6%), only the interface would be strained and the other part of thin films would be relaxed[32]. The strain relaxation is accompanied by a breakup into small domains of Fe_3O_4 with a wide distribution of the domain size, which can also lower the Verwey transition temperature. Thus, the difference between samples with different growth temperature can be explained by the different strain status. Samples grown at 450°C which has a higher Verwey transition temperature could be more relaxed and samples with T_{growth} = 550°C could be more strained.

4.4.5 Discussion

We discussed the magnetization behavior which will be influenced by the Verwey transition. In addition, the Verwey transition can be influenced by the stoichiometry of Fe_3O_4 thin films and the strain that appears during deposition (i.e. due to the lattice mismatch). In order to analyze the influence of two parameters, it is reasonable to take samples with T_{growth} = 400°C and 550°C as comparison for further experiments.

4.5 Electric properties

We looked into the Verwey transition and magnetoresistance.

4.5.1 Experiment details

The dependence of the resistance of thin films on temperature and magnetic field are measured in a Quantum Design Dynacool-PPMS (Physical Properties Measurement System). In our experiments, resistance versus temperature (R(T)) curves are recorded with cooling and warming between 10K with 300K with zero magnetic field. The magnetoresistance versus field hysteresis loops (MR(H)) are also recorded at different temperature T=90-300K in the range of H=±2T. All the measurements are done in two ways: with magnetic field perpendicular and parallel to the thin film.

4.5.2 Resistance versus temperature

The resistance of Fe_3O_4 thin films with magnetic field parallel with the thin films are plotted in Figure 4.13(a). With decreasing measuring temperature, all the samples show an increase in resistance. There is a clear transition around 120K which is the Verwey transition: a first order metal-insulator transition. However, the discontinuous transition is not clear, thus we calculate the accurate Verwey transition temperature.

The resistivity is calculated by [33]:

$$\rho = \frac{\pi}{ln2 * thickness} * \frac{Voltage}{Current} \qquad (4-2)$$

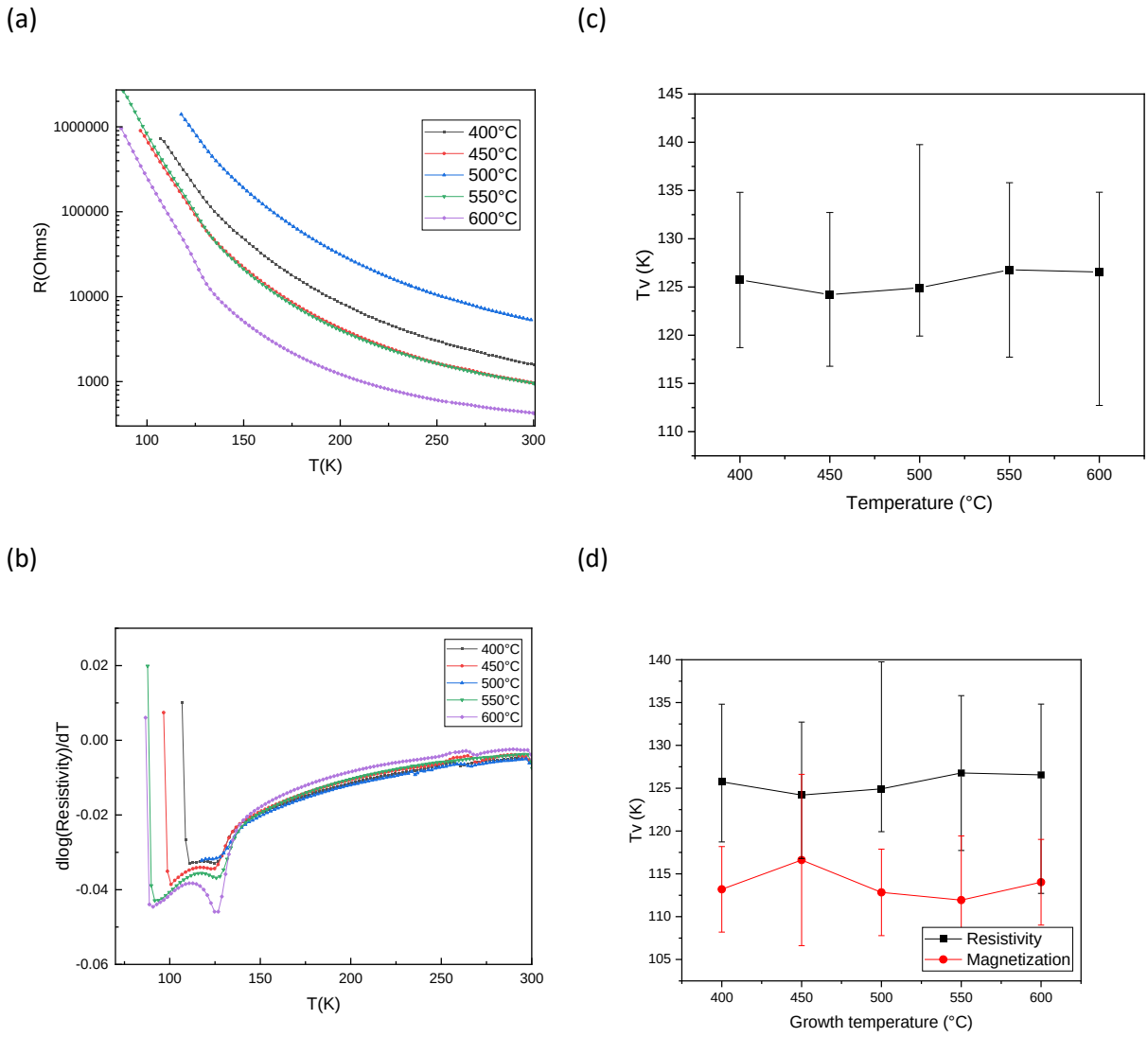

Figure 4.13 (a)Resistance versus temperature, (b) dlog(Resistivity)/dT for Fe_3O_4 thin films grown at 400, 450, 500, 550, 600° and Verwey transition temperatures calculated from (c) resistivity and (d) resistivity and magnetization

According to dlog(Resistivity)/dT as shown in Figure 4.13(b), we can find the local maximum around 120K which is Verwey transition temperature.

When T_{growth}=600°C, the sample shows the clearest transition which indicates good stoichiometry. When T_{growth}=400, 500°C, the Verwey transition appears at the lowest temperature and the transition is the most unclear, which suggests too much oxygen content.

The accurate Verwey transition temperatures are plotted in Figure 4.13(c). Different from the Verwey transition calculated from magnetization, the results are closer to the bulk value (124K). This could originate from the difference in measuring instruments. Figure 4.13(d) compares the

Verwey transition temperature calculated from M(T) and R(T). Though the Verwey transition temperature calculated from magnetization (red curve) is lower than the one calculated from resistivity (black curve), the error caused by the transition width is rather large. Besides, both Verwey transition temperatures from two devices of sample grown at 450°C are the nearest to the bulk value 124K and both of sample grown at 550°C are most far away from the bulk value. This may be caused by the different strain status: Fe_3O_4 thin film grown at 450°C is more relaxed and the one at 550°C is more strained.

4.5.3 In-plane magnetoresistance

Apart from the R(T), we are more interested in the magnetoresistance of Fe_3O_4 thin films. Most metals show a positive magnetoresistance which means the magnetic field can cause an increase of resistance[7]. This is because of the electrons take different paths with applied magnetic field, which causes more scattering and leads to the increased magnetoresistance. However, a special negative magnetoresistance was reported in Fe_3O_4. Yamada firstly reported the possible principle of negative magnetoresistance: with applying magnetic field, the fluctuation of spins is suppressed which leads to a decrease of the resistance[34]. However, the principle of negative magnetoresistance in Fe_3O_4 thin films is not yet fully understood and explained. In our measurements, Fe_3O_4 thin films also show negative magnetoresistance as shown in Figure 4.14 (a) – (e) with the growth temperature from 400°C to 600°C. It was reported that magnetoresistance of Fe_3O_4 is associated with magnetic field, strongly influenced by anti-phase boundaries[32,35,36]. Magnetoresistance decreases with applying magnetic field representing the field-induced alignment of the magnetic domains. This means neighboring antiphase boundary magnetic moments align in the direction of the field, resulting in reduced resistance.

Besides the influence of the magnetic field, magnetoresistance is also influenced by the measuring temperature. When temperature is higher than 120K (around Verwey transition temperature), with the lower measuring temperatures, the magnetoresistance increases significantly. However, when temperature is lower than 120K, the change between different temperature is slight. This different dependency of temperature is because of the influence of

temperature on magneto crystallin anisotropy is smaller when temperature is smaller than Verwey transition temperature.

We also observed a non-closed loop which could because of the anisotropy of the alignment which also occurs in others' study[37]. The principle is still need to study. However, after repeating the measurement for several times, this non-closed behavior disappears

In the in-plane magnetoresistance, there are maximums at positive and negative magnetic field and we can plot it verses the measuring temperature for samples grown at different temperature as shown in Figure 4.14 (f).

We found consistency with the coercivity measurements. The magnetization and magnetoresistance changing with magnetic field is shown in Figure 4.15. For all the measuring temperature, there is a clear consistency between the field at maximum of magnetoresistance and the coercivity which is also found in another study[38].

4.5.5 Out-of-plane magnetoresistance

Complementary to the in-plane electric behavior, we observed the out-of-plane magnetoresistance with magnetic field perpendicular to the thin films which is shown in Figure 4.16. Magnetoresistance with the in-plane field shows a sharp increase at low field but a slow growth under high field. Unlike the in-plane behavior, the out-of-plane magnetoresistance increases slightly at low field and more linearly with higher field.

4.5.6 Discussion

With T_{growth}=550 and 600°C Fe_3O_4 shows a clear Verwey transition. All the Verwey transition temperature calculated from resistance versus temperature are around the bulk value which indicates the oxygen stoichiometry is within the critical value. We also observed the different behavior of magnetoresistance between magnetic field parallel or perpendicular to the thin films. The in-plane magnetic field at maximum magnetization shows the same tendency as the coercivity measurements.

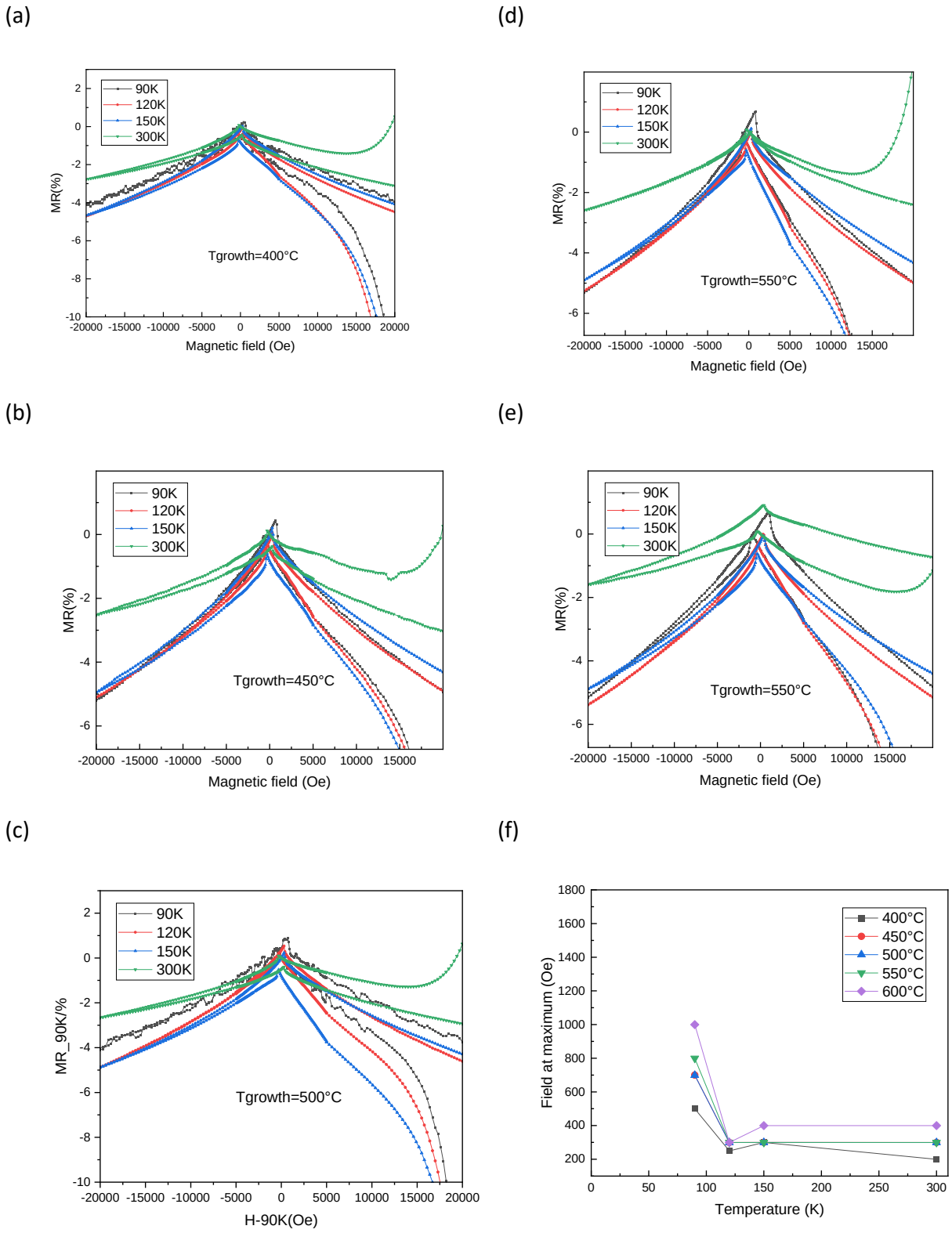

Figure 4.14 Magnetoresistance at different measuring temperature for Fe_3O_4 thin films grown at temperature (a) 400°C, (b) 450°C, (c) 500°C, (d) 550°C, (e) 600°C. (f) Field at maximum magnetoresistance vs. growth temperature.

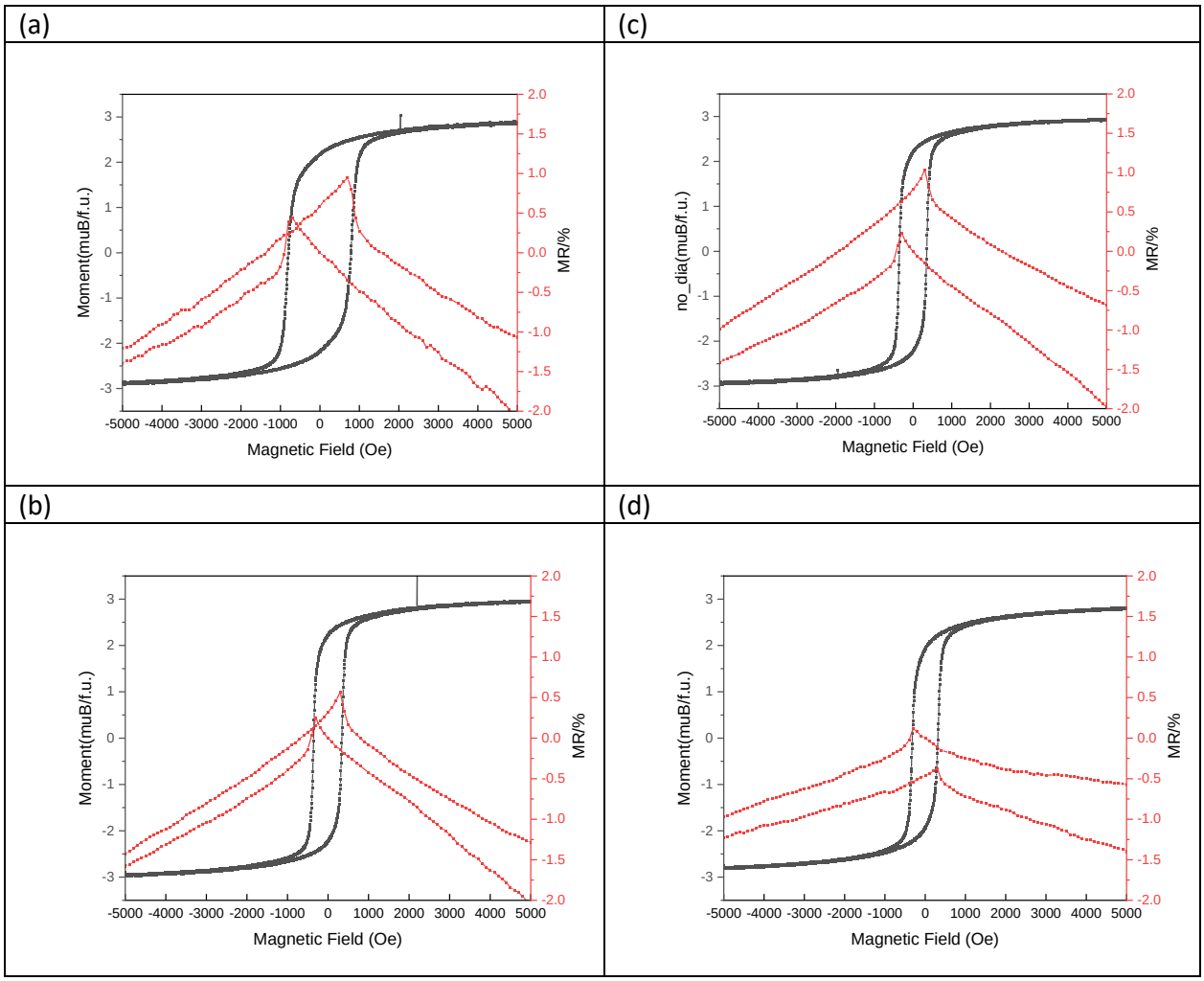

Figure 4.15 In-plane magnetoresistance (red curves) and magnetization (black curves) versus magnetic field for sample grown at 450°C at measuring temperature of (a)90K, (b)120K, (c)150K and (d)300K.

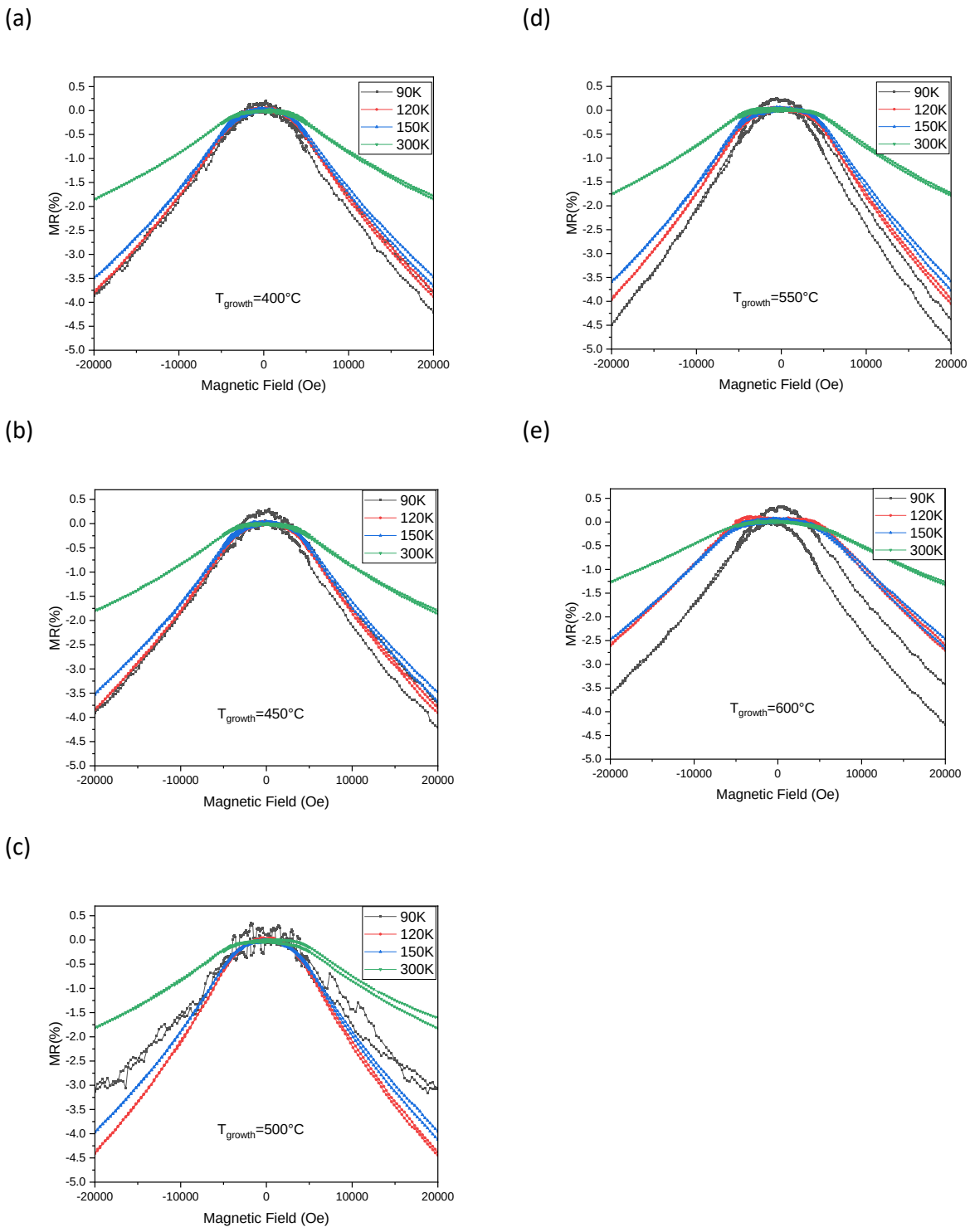

Figure 4.16 Out-of-plane magnetoresistance at different measuring temperature for Fe_3O_4 thin films grown at temperature (a) 400°C, (b) 450°C, (c) 500°C, (d) 550°C, (e) 600°C.

5 Summary

This project is a initial study on optimizing the growth parameter of Fe_3O_4 thin films on the YSZ substrate deposited by PLD. In this project, we have managed to find the best laser fluency to grow Fe_3O_4 thin films which showed a relatively homogeneous surface with thickness around 40nm and a good single crystallinity. Based on this laser fluency, we performed measurements on samples grown at different growth temperature.

From AFM and XRR, we observed the relatively smooth surface with low roughness which indicates a good quality thin film. From XRD measurements we observed all peaks of Fe_3O_4 in the same direction which indicates the single crystallinity. In addition, Laue oscillations appear for all the samples which indicates the good crystallinity under this optimized laser fluency.

We observed the saturation magnetization lower than the bulk value because of the assumed presence of anti-phase boundaries. The changing of coercivity is associated with the transition of the magnetic easy axis induced by the changing of crystal lattice structure when crossing the Verwey transition temperature.

The Verwey transition temperature was calculated from the magnetization and resistance. As a good indicator of oxygen stoichiometry, we find that the Verwey transition temperature calculated by the magnetization is much lower than the bulk which can be affected by the wide transition width for both measurements. By combing two kinds of measurements, we find that there are common behaviors: the sample grown at $450\,^{\circ}C$ shows the Verwey transition temperature closest to the bulk value and the one grown at 550°C the most far away. This indicates the different strain state among different growth temperatures.

For electrical property measurements, negative magnetoresistance is observed for all measuring temperatures in both in-plane and out-of-plane directions.

6 Outlook

In this project, we optimized the growth parameter of Fe_3O_4 and observed different strain and oxygen stoichiometry for different growth temperatures. This optimization is a good foundation to now grow Fe_3O_4 on $SrTiO_3$ (STO) substrates, which has a rather more complicated oxygen supply behavior.

Based on the optimized growth temperature, we will investigate the properties of Fe_3O_4 thin films on STO substrates. In addition, we will attempt to tune the properties of the Fe_3O_4 thin films. First, we will try to tune the properties by annealing and observe the changing of the oxide phase by XRD. Then, we will try to tune the properties by applying an electric field. Here, the changing of lattice structure and magnetic properties will be observed by wide-angle X-ray scattering (WAXS) and SQUID respectively. Finally, we will analyze the influence of oxide substrates on Fe_3O_4 thin films by using differently terminated STO substrates.

Reference

1 Hirohata, A. *et al.* Review on spintronics: Principles and device applications. *Journal of Magnetism and Magnetic Materials* **509**, 166711, doi:https://doi.org/10.1016/j.jmmm.2020.166711 (2020).

2 Zhang, Z. & Satpathy, S. Electron states, magnetism, and the Verwey transition in magnetite. *Physical Review B* **44**, 13319-13331, doi:10.1103/PhysRevB.44.13319 (1991).

3 Blaney, L. Magnetite (Fe3O4): Properties, synthesis, and applications. (2007).

4 Fonin, M., Dedkov, Y., Pentcheva, R., Rüdiger, U. & Güntherodt, G. Magnetite: A search for the half-metallic state. *Journal of physics. Condensed matter : an Institute of Physics journal* **19**, 315217, doi:10.1088/0953-8984/19/31/315217 (2007).

5 Fleet, M. The structure of magnetite. *Acta Crystallographica Section B* **37**, 917-920, doi:doi:10.1107/S0567740881004597 (1981).

6 Friák, M., Schindlmayr, A. & Scheffler, M. Ab initio study of the half-metal to metal transition in strained magnetite. *New J. Phys.* **9**, doi:10.1088/1367-2630/9/1/005 (2007).

7 Blundell, S. Magnetism in condensed matter: oxford master series. *Condensed Matter Physics (Oxford Series Publications, 2001)*, 29 (2001).

8 Hamed, M. H. A. Interface Functionalization of Magnetic Oxide Fe3O4/SrTiO3 Heterostructures. Report No. 395806535X, (Elektronische Eigenschaften, 2021).

9 Anderson, P. Antiferromagnetism. Theory of superexchange interaction. *Physical Review* **79**, 350 (1950).

10 Kanamori, J. Superexchange interaction and symmetry properties of electron orbitals. *Journal of Physics and Chemistry of Solids* **10**, 87-98 (1959).

11 Goodenough, J. B. Theory of the role of covalence in the perovskite-type manganites [La, M (II)] Mn O 3. *Physical Review* **100**, 564 (1955).

12 Verwey, E. Electronic conduction of magnetite (Fe 3 O 4) and its transition point at low temperatures. *Nature* **144**, 327-328 (1939).

13 Verwey, E. & Heilmann, E. Physical properties and cation arrangement of oxides with spinel structures I. Cation arrangement in spinels. *The Journal of Chemical Physics* **15**, 174-180 (1947).

14 Aragón, R., Buttrey, D. J., Shepherd, J. P. & Honig, J. M. Influence of nonstoichiometry on the Verwey transition. *Physical Review B* **31**, 430-436, doi:10.1103/PhysRevB.31.430 (1985).

15 Chase, M. W. NIST-JANAF thermochemical tables for oxygen fluorides. *Journal of physical and chemical reference data* **25**, 551-603 (1996).

16 Molina-Reyes, J. *et al.* Physical and electrical characterization of yttrium-stabilized zirconia (YSZ) thin films deposited by sputtering and atomic-layer deposition. *Journal of Materials Science: Materials in Electronics* **29**, 15349-15357, doi:10.1007/s10854-018-8909-3 (2018).

17 Gilks, D. *et al.* Structural study of Fe3O4 (111) thin films with bulk like magnetic and magnetotransport behaviour. *Journal of Applied Physics* **115**, 17C107 (2014).

18 Herrmann, M. G. *Crystal structures and vibrational properties of chalcogenides: the role of temperature and pressure*. (Forschungszentrum Jülich GmbH, Zentralbibliothek, Verlag, 2019).

19 Glavic, A. *Multiferroicity in oxide thin films and heterostructures*. Vol. 45 (Forschungszentrum Jülich, 2012).

20 Biermanns, A. X-Ray-Reflectometry.

21 Björck, M. & Andersson, G. GenX: an extensible X-ray reflectivity refinement program utilizing differential evolution. *Journal of Applied Crystallography* **40**, 1174-1178 (2007).

22 Stan, C., Beavers, C., Kunz, M. & Tamura, N. X-Ray Diffraction under Extreme Conditions at the Advanced Light Source. *Quantum Beam Science* **2**, doi:10.3390/qubs2010004 (2018).

23 Kittel, C. Introduction to solid state physics. (1976).
24 Reddy, Y. K. V., Wolfman, J., Autret-Lambert, C., Gervais, M. & Gervais, F. Strain relaxation of epitaxial (Ba0.6Sr0.4)(Zr0.3Ti0.7)O3 thin films grown on SrTiO3 substrates by pulsed laser deposition. *Journal of Applied Physics* **107**, 106101, doi:10.1063/1.3380528 (2010).
25 Quantum Design PPMS manual.
26 Hamed, M. H., Mueller, D. N. & Müller, M. Thermal phase design of ultrathin magnetic iron oxide films: from Fe 3 O 4 to γ-Fe 2 O 3 and FeO. *Journal of Materials Chemistry C* **8**, 1335-1343 (2020).
27 Nečas, D. & Klapetek, P. Gwyddion: an open-source software for SPM data analysis. *Open Physics* **10**, 181-188 (2012).
28 Kiessig, H. Untersuchungen zur totalreflexion von röntgenstrahlen. *Annalen der Physik* **402**, 715-768 (1931).
29 Bertotti, G. *Hysteresis in Magnetism: For Physicists, Materials Scientists, and Engineers*. (Elsevier Science, 1998).
30 Bohra, M., Agarwal, N. & Singh, V. A short review on Verwey transition in nanostructured Fe3O4 materials. *Journal of Nanomaterials* **2019** (2019).
31 Brabers, V., Walz, F. & Kronmüller, H. Impurity effects upon the Verwey transition in magnetite. *Physical Review B* **58**, 14163 (1998).
32 Liu, X., Rata, A., Chang, C., Komarek, A. & Tjeng, L. Verwey transition in Fe 3 O 4 thin films: Influence of oxygen stoichiometry and substrate-induced microstructure. *Physical Review B* **90**, 125142 (2014).
33 Battiston, G. A., Gerbasi, R., Porchia, M. & Marigo, A. Influence of substrate on structural properties of TiO2 thin films obtained via MOCVD. *Thin Solid Films* **239**, 186-191, doi:https://doi.org/10.1016/0040-6090(94)90849-4 (1994).
34 Yamada, H. & Takada, S. Magnetoresistance of antiferromagnetic metals due to s-d interaction. *Journal of the Physical Society of Japan* **34**, 51-57 (1973).
35 Liu, X., Chang, C., Tjeng, L., Komarek, A. & Wirth, S. Large magnetoresistance effects in Fe3O4. *Journal of Physics: Condensed Matter* **31**, 225803 (2019).
36 Reddy, K., Padture, N. P., Punnoose, A. & Hanna, C. Magnetoresistance characteristics in individual Fe3O4 single crystal nanowire. *Journal of Applied Physics* **117**, 17E115 (2015).
37 Ziese, M. & Blythe, H. Magnetoresistance of magnetite. *Journal of Physics: Condensed Matter* **12**, 13 (2000).
38 Coey, J., Berkowitz, A., Balcells, L., Putris, F. & Parker, F. Magnetoresistance of magnetite. *Applied Physics Letters* **72**, 734-736 (1998).